Wave interactions and the transition to chaos of baroclinic waves in a thermally driven rotating annulus

By W.-G. Früh† and P. L. Read

Sub-Department of Atmospheric, Oceanic, and Planetary Physics, Department of Physics, University of Oxford, Oxford OX1 3PU, UK

Contents

A series of laboratory experiments is presented investigating regular and chaotic baroclinic waves in a high-Prandtl number fluid contained in a rotating vessel and subjected to a horizontal temperature gradient. The study focuses on nonlinear aspects of mixed-mode states at moderate values of the forcing parameters within the

† Present address: Department of Physics and Astronomy, University of Edinburgh, Mayfield Road, Edinburgh EH9 3JL, UK.

Phil. Trans. R. Soc. Lond. A (1997) **355**, 101–153

regular wave regime. Frequency entrainment and phase locking of resonant triads and sidebands were found to be widespread. Cases were analysed in phase space reconstructions through a singular value decomposition of multi-variate time series. Four forms of mixed-mode states were found, each in well-defined regions of parameter space: (1) a nonlinear interference vacillation associated with strong phase locking through higher harmonics; (2) a modulated amplitude vacillation showing strong phase coherence in triads involving the long wave; (3) an intermittent bursting of secondary modes; (4) an attractor switching flow, where the dominant wave number switched at irregular intervals between two possible wave numbers.

Many of the mixed-mode states are suggested to arise from homoclinic bifurcations, whereas no secondary Hopf bifurcations were found. One of the postulated homoclinic bifurcations was consistent with a bifurcation through intermittency. The bifurcation sequences, however, were strongly affected by phase locking between different wave number components and frequency locking between drift and modulation frequencies. When all free frequencies were locked, the flow reduced to a limit cycle which subsequently became unstable through an incomplete period-doubling cascade. The only observed case of torus-doubling was also associated with strong phase locking.

Most of the observed regimes were consistent with low-dimensional dynamics involving a limited number of domain-filling modes, which can be represented in phase space reconstructions and characterized by invariants such as attractor dimensions and the Lyapunov exponents. Some flows associated with a weak structural vacillation, however, were not consistent with low-dimensional dynamics. It appeared rather that they were the result of spatially localized instabilities consistent with high-dimensional dynamics, which can be parametrized as stochastic dynamics.

---

1. Introduction

In the mid-latitude atmosphere baroclinic waves are among the most energetic large-scale phenomena contributing to the poleward transport of heat and momentum, and it is widely accepted that fully developed nonlinear baroclinic waves have a significant effect on the atmospheric circulation and its predictability. These wave-like perturbations of the westerly winds in the middle latitudes grow from an instability of the rapidly rotating atmosphere subjected to a horizontal temperature gradient caused by the differential solar heating.

One system to study baroclinic waves in laboratory experiments is the thermally driven rotating annulus (Hide & Mason 1975). In this system an upright cylindrical fluid annulus is differentially heated in the horizontal and rotated about its vertical axis of symmetry (see figure 1). With the imposed temperature difference and the rotation rate of the apparatus a stability parameter Θ and the Taylor number $\mathcal{T}$, the two principal non-dimensional parameters, can be defined. The stability parameter, sometimes referred to as a Burger number or thermal Rossby number and related to the rotational Froude number, is defined by

$$\Theta \equiv \frac{g\alpha\Delta T d}{\Omega^2(b-a)^2}, \tag{1.1}$$

where g is the acceleration due to gravity, α the volume expansion coefficient, ΔT the imposed horizontal temperature difference, Ω the rotation rate, d the depth, and

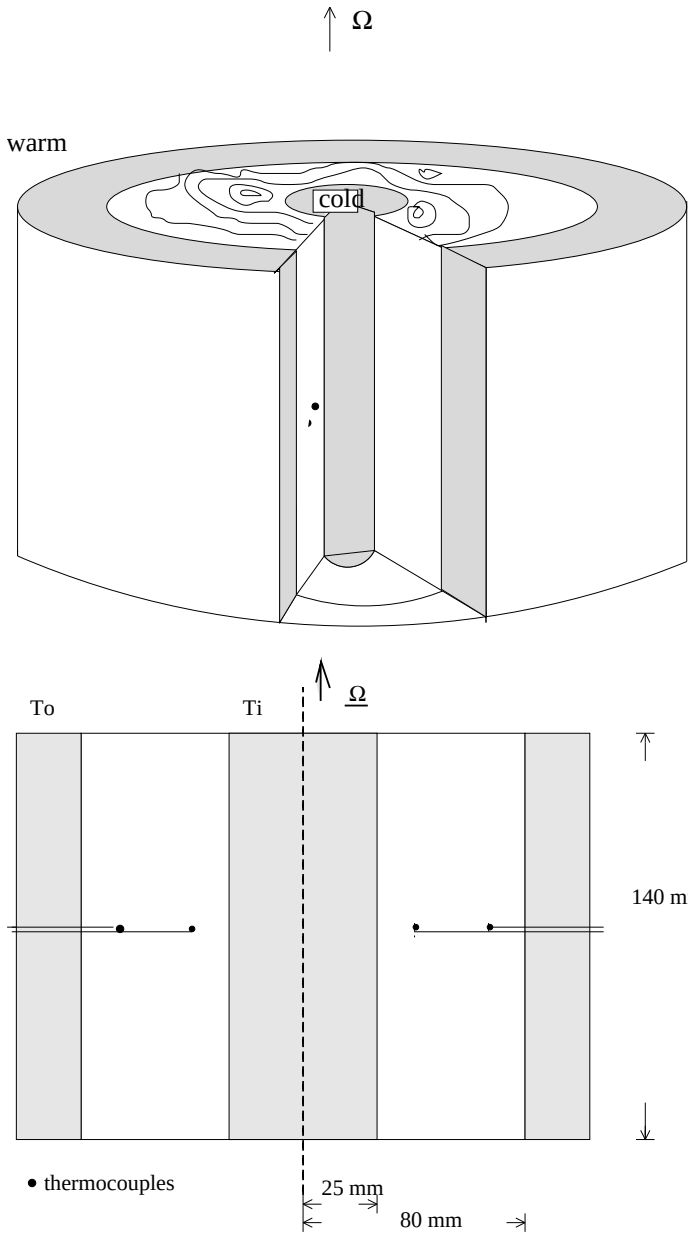

Figure 1. Schematic diagram and cross-section of the rotating annulus.

a and b the inner and outer radius of the annulus as shown in figure 1*b*. The Taylor number is usually defined by

$$\mathcal{T} \equiv \frac{4\Omega^2(b-a)^5}{\nu^2 d}, \tag{1.2}$$

where ν is the kinematic viscosity.

The resulting flows show a wide variety of distinct regimes depending upon the experimental parameters. Besides steady axisymmetric flows on one side and spatially

irregular, aperiodic flows, the so-called 'geostrophic turbulence', on the other, the regimes at intermediate parameter values include flows of spatially regular waves drifting through the annulus which can be steady, quasi-periodic, or aperiodic in time. The main variants of time-dependent regular waves are usually classified as amplitude vacillation (AV) and structural or shape vacillation (SV) (Hide & Mason 1975; Pfeffer *et al.* 1980). AV is characterized by the periodic growth and decay of the wave amplitude with little change in wave shape, resulting in an oscillatory heat transport across the annulus, while in SV it is the wave shape rather than the total amplitude which changes, resulting in only weakly varying heat transport across the annulus. Experiments with the rotating annulus have so far concentrated on phenomena with timescales from $O(10)$ rotation periods—a few minutes—which is a typical timescale of the vacillations, to $O(100)$ rotation periods, the range of typical drift periods. More recently, however, oscillations on significantly longer timescales have been found. Read *et al.* (1992) (in the following referred to as RBJS) observed a chaotic mixed-wave state, a modulated amplitude vacillation (MAV) with a modulation timescale of up to 1000 rotation periods, well within the regular wave regime, though precise parametric boundaries and bifurcation sequences were not determined.

The work presented in this paper was motivated by the observations by RBJS of this chaotic, low-frequency MAV regime, which they suggested arose from nonlinear wave interactions apparent in the phase coherence of the dominant wave mode and its sidebands. As well as this MAV, a number of novel types of very-low frequency oscillations and mixed-mode states were found at parameter values close to the MAV regime. The experiment and the methods to analyse the data are presented in § 2, with emphasis on the method to evaluate the strength of the phase locking. The presentation of the results is divided into the description of the general results in § 3 and the results from specific subregimes in § 4–7. In § 8 possible explanations for the occurrence of mixed-mode states and the low-frequency variability will be discussed, and the main points are summarized in § 9.

2. Experimental apparatus and procedures

(*a*) *Apparatus*

Experiments were performed using a conventional rotating annulus, which was—apart from the experimental control and instrumentation—identical to the apparatus used by Hignett *et al.* (1985) and RBJS. A schematic drawing and a cross-section of the annulus are shown in figure 1. The vertical side walls consisted of two coaxial brass cylinders with boundaries at radii $a = 25$ mm and $b = 80$ mm which were kept at different, constant temperatures, while the horizontal lid and base were thermally insulating. The fluid depth was $d = 140$ mm. The annulus was mounted on a turntable such that its vertical axis of symmetry coincided with the axis of rotation. To investigate low-frequency behaviour the experimental conditions needed to be maintained constant for a long time (a single experiment lasted typically 24 h). This was achieved by a computerized experimental control system; the accuracy of the turntable rotation was better than 1 part in 10^5 over timescales of a few minutes, without any detectable variation over timescales longer than 1 h, and the wall temperatures could be maintained to within ± 0.01 K. The system also offered fully automated parameter control with smoothly varying experimental parameters. With this technique it was possible to cover a range of parameters $\mathcal{T}$ and Θ while keep-

ing interruptions to the equilibrated flow to a minimum. The working fluid used was the same water/glycerol solution as RBJS, with *ca.* 17% by volume of glycerol and a Prandtl number of $Pr = 26.7$ at 20 °C. The temperatures of the fluid interior and the side walls were measured using copper-constantan thermocouples with a sensitivity of $40\,\mu\mathrm{V\,K^{-1}}$. Two configurations of thermocouple arrangements were used, a single thermocouple ring and a double ring. In the single ring, 32 thermocouples were equally spaced in azimuth at mid-height ($z = 70$ mm) and mid-radius ($y = (r-a)/(b-a) = 1/2$). With this configuration, which was also used by RBJS, the azimuthal wave number spectrum could be obtained by Fast Fourier Transform techniques. In the second configuration, 64 thermocouples were arranged in two concentric thermocouple rings of 32 thermocouples each, again equally spaced in azimuth. Both rings were at mid-height, one at $y = 1/4$ and the other at $y = 3/4$. With these two rings some information on the radial structure could be obtained besides the azimuthal wave number spectrum. The experiment's dimensions, fluid properties, and sensors are listed in table 1.

(*b*) *Experimental procedure*

Following RBJS, the range of parameters investigated was restricted to a range of $8\times10^5 < \mathcal{T} < 2\times10^7$ and $0.05 < \Theta < 1.1$. Due to the timescales involved, each of the experiments for one pair of $\mathcal{T}$ and Θ lasted for 20 h, or typically *ca.* $20000\tau_0$ where τ_0 is the rotation period of the annulus. During these 20 h either all thermocouples were scanned at 12 s intervals or, to achieve a better temporal resolution, only a subset of the thermocouples was used; typically 16 thermocouples at $3s$ intervals. After the 20 h measuring period the Taylor number $\mathcal{T}$ was gradually increased by about 5% over a period of 2 h, while Θ was kept constant. Following the change of parameters the flow was allowed to settle down for another 2 h before the next 20 hour-long measuring period began. Each set of experiments performed in this way for a fixed value of Θ contained 10 to 15 experiments covering a range of $\Delta\mathcal{T}$ of 3×10^6 to 10^7. For some sets of experiments $\mathcal{T}$ was kept fixed while Θ was gradually increased in the same manner as described above.

The same procedure was also applied for *decreasing* values of $\mathcal{T}$ or Θ, respectively. This was done to detect possible hysteresis in flow transitions and multiple equilibria.

(*c*) *Data analysis*

(i) *Fourier analysis*

For the analysis of the data two methods were used: spatial Fourier transform and multi-channel singular systems analysis (M-SSA). With fast Fourier transform techniques applied to each thermocouple ring, the azimuthal temperature structure of the flow field could be decomposed into the amplitude and phase of normal modes. The amplitude information was used to classify the flow type. A clear distinction between AV and SV was possible by comparing the amplitude of the dominant wave mode of the outer ring with that of the inner ring. If there was no temporal phase shift between the vacillation detected at the two rings then the gravest radial mode (and/or higher odd modes) dominated the flow indicating AV, whereas a temporal phase shift of approximately π indicated a dominating second radial mode (and/or higher even modes), which is a characteristic of structural vacillation (cf. Pfeffer *et al.* 1980).

Table 1. (*a*) *Annulus dimensions,* (*b*) *typical experimental conditions,* (*c*) *fluid properties at* 20 °C, *and* (*d*) *sensors*

	symbol	value	precision	units
(*a*) Annulus dimensions				
inner cylinder radius	a	25.0	±0.1	mm
outer cylinder radius	b	80.0	±0.1	mm
cavity depth	d	140.0	±0.2	mm
levelling on turntable			$\pm 10^{-4}$	rad
centring on turntable			±1.0	mm
(*b*) Typical experimental conditions				
rotation rate	Ω	1...3	$\pm 10^{-5}$	rad s^{-1}
mean temperature	$\langle T \rangle$	20.00	±0.02	°C
temperature difference	ΔT	3...20	±0.02	K
(*c*) Glycerol/water with volume ratio ≈ 17%				
density	ρ	1098	±1	kg m^{-3}
kinematic viscosity	ν	3.2×10^{-6}		m^2 s^{-1}
thermal conductivity	κ	1.2×10^{-7}		m^2 s^{-1}
Prandtl number	$Pr \equiv \nu/\kappa$	26.7		
volume expansion	α	4.0×10^{-4}		K^{-1}
(*d*) Sensors				
thermocouple ring	T	18...23	±0.01	°C
wall temperatures	T	10...30	±0.01	°C
rotation rate	Ω	1...2.5	$\pm 3 \times 10^{-6}$	rad s^{-1}

(ii) *Phase locking*

Spatial phase relationships of the wave modes with respect to each other are a clear sign of nonlinear wave interactions, the simplest of which is the three-wave resonance (cf. Craik 1985). As Bretherton (1964) and Plumb (1977) showed, three wave modes constitute a resonantly interacting wave triad if the sum or difference of their wave vectors, $\boldsymbol{k}_i$, is zero, and if the angular frequencies of the wave drift, ω_i, add up to a frequency much smaller than the average drift, $\langle \omega \rangle$:

$$\boldsymbol{k}_m \pm \boldsymbol{k}_{m'} \pm \boldsymbol{k}_{m''} = 0 \tag{2.1}$$

and

$$\omega_m - \omega_{m'} - \omega_{m''} \ll \langle \omega \rangle. \tag{2.2}$$

The drift frequencies of finite-amplitude waves depended, among other factors, on the wave amplitude, and thus time-dependent flows may intermittently satisfy the resonance condition (2.2). Integrating (2.2) over time yields

$$\varphi_{m-m'-m''} \equiv \phi_m - \phi_{m'} - \phi_{m''} \approx \text{const.} \tag{2.3}$$

Measuring the degree to which $\varphi_{m-m'-m''}$ clusters around a constant value shows the importance of the particular wave triad with waves $\boldsymbol{k}_m$, $\boldsymbol{k}_{m'}$, and $\boldsymbol{k}_{m''}$. A 'locking density', $\rho_{m-m'-m''}$, may be defined over the data set, which gives information about the time-averaged phase locking: strong phase coherence would result in a strong peak at the preferred value of φ, while no phase coupling would give a flat density function over its entire range $0 \ldots 2\pi$. In Appendix A a derivation of $\rho_{m-m'-m''}$ is given, together with a description of how to evaluate the locking density.

A higher-order interaction is the sideband interaction (Plumb 1977), first discussed in the breakdown of surface waves by Benjamin & Feir (1967), in which case the dominant mode, m, and its sidebands $m \pm \delta$ travel at the same phase speed. In the annulus with a discrete azimuthal wave spectrum the sidebands of mode m are $m \pm 1$, and the resonance condition for this wave interaction mechanism is

$$2\omega_m - \omega_{m-1} - \omega_{m+1} \ll \langle\omega\rangle. \tag{2.4}$$

It follows that this equation, integrated over time, leads to

$$\Phi_m = 2\phi_m - \phi_{m-1} - \phi_{m+1}, \tag{2.5}$$

where Φ_m is approximately constant. As in the triad phase locking a sideband locking probability density, ρ_m, can be defined as a measure of the time-averaged strength of the wave coupling by this mechanism with equation (A 4), but using Φ_m instead of $\varphi_{m-m'-m''}$.

(iii) *Phase space reconstruction*

In order to get information on the flow as a finite-dimensional dynamical system, phase portraits were reconstructed using the temperature measurements from a subset of the entire thermocouple ring arrangement. The reconstructions employed a form of singular systems analysis (SSA), or singular value decomposition (SVD), in the form developed by Broomhead & King (1986) and implemented for multivariate (M-SSA) data by Read (1993). Apart from the representation of the flow in phase portraits, Poincaré sections and return maps, invariants of the flow were calculated from the M-SSA phase space reconstruction, namely the attractor dimension after Grassberger & Procaccia (1983) and the largest Lyapunov exponent after Wolf *et al.* (1985).

3. Results

(*a*) *The regime diagram*

The experiments presented in this study were performed over the range in $\mathcal{T}$ and Θ of $6 \times 10^5 \leqslant \mathcal{T} \leqslant 2 \times 10^7$ and $0.05 \leqslant \Theta \leqslant 1.1$, which generally resulted in spatially regular waves with relatively low azimuthal wave numbers. All observed flows were dominated by waves with wave numbers $m \leqslant 4$. Figure 2 shows a regime diagram of the parameter space investigated. The classification of the flow types was made on the basis of a spatial Fourier transform of the temperature records from

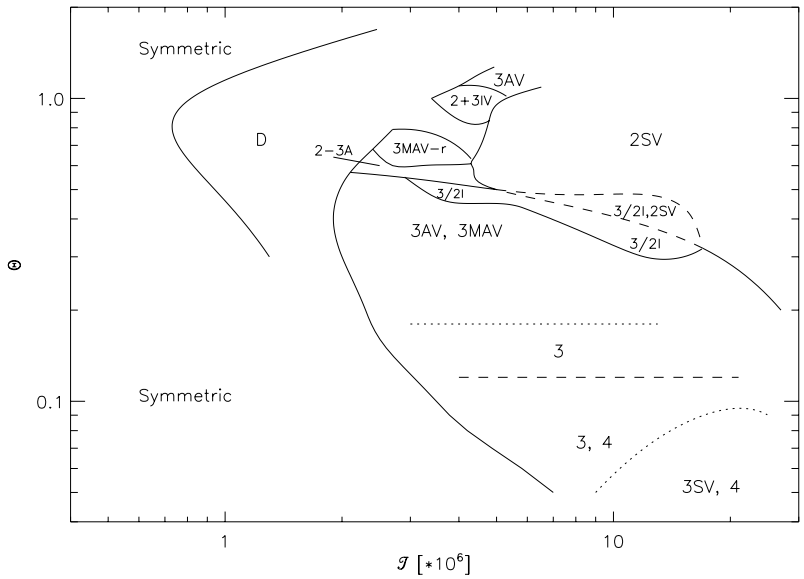

Figure 2. Regime diagram, showing all regimes observed over the range in $\mathcal{T}$ and Θ investigated. The dashed lines indicate hysteresis. Where more than one flow type was found, all types are listed separated by commas. Since the onset of vacillation is difficult to determine, only an approximate indication is given by the dotted lines. The abbreviations are listed in table 2.

the thermocouple rings, which resulted in time series of the amplitudes and phases of zonal wave modes. The different flows were achieved by changing the parameters smoothly and slowly across the parameter space as described in § 2 *b*. The first part of this section will present the general structure of the regime diagram as well as some features common to several different flow types. It was found that the phase velocities of the dominant wave mode generally followed a well defined functional dependence on the control parameters, $\mathcal{T}$ and Θ, but that they were independent of wave number, as discussed further in § 3 *b*. This section of general results is followed by a discussion of specific subregimes in §§ 4–7.

The general features of the regime diagram in figure 2 are not only in good quantitative agreement with the study by RBJS, who used a fluid with an identical Prandtl number ($Pr \approx 26$), but are also in qualitative agreement with annulus experiments which used fluids with lower Prandtl numbers (James *et al.* 1981). The flow types in the regime diagram, which are introduced in the following paragraphs, are summarized in table 2. Experiments, which will be referred to in the following sections by their labels (a) to (m), are listed in table 3.

The simplest flow, denoted *symmetric* in the regime diagram, is a steady purely zonal flow with a vertical shear. The shear flow is in thermal wind balance with the imposed temperature gradient. In the upper symmetric regime, for large values of Θ, the stratification suppresses instability. In the lower symmetric regime, at small $\mathcal{T}$ and small Θ, diffusive effects stabilize the zonal flow. The transitions from these two regimes to baroclinic waves form the characteristic anvil shape in the regime diagram, which has been extensively studied (Hide & Mason 1975).

The wave regimes are denoted by their dominant wave number, together with abbreviations indicating their temporal behaviour. In flows which are characterized by

Table 2. *Summary of the flow types shown in the regime diagram*

term	description
symmetric	purely zonal flow with vertical shear
D	dispersive weak waves with irregularly fluctuating wave amplitudes
2	steady $m = 2$ wave
2SV	structural vacillation of $m = 2$
3	steady $m = 3$ wave
2+3IV	dispersive steady waves $m = 2$ and $m = 3$
3AV	amplitude vacillation of $m = 3$
3MAV	modulated amplitude vacillation of $m = 3$
3MAV-r	3MAV with reversed phase drift
3/2I	3MAV with intermittent bursts of $m = 2$
2-3A	3MAV alternating with 2SV
3SV	structural vacillation of $m = 3$
4MAV	modulated amplitude vacillation of $m = 4$

more than one wave mode, the two most energetic wave numbers are used to label the regime. A simple number, e.g. 3, denotes a steady wave pattern with the corresponding zonal wave number, $m = 3$, which drifted with a well defined frequency along the annular channel, while its shape and amplitude remained relatively constant over time. Phase space reconstructions from temperature time series measured at fixed locations in the fluid gave limit cycles in this regime. One tends to observe lower wave numbers towards higher Θ or higher $\mathcal{T}$, although the existence of multiple equilibria is widespread and is a well known phenomenon in this system (Hide & Mason 1975), in the sense that more than one wave number or flow type can be observed under identical parameter conditions. In figure 2 this is shown by listing the observed flow types separated by commas, as in '3,4MAV', for example. Apart from the choice of the parameters, the observed flow depends largely on the initial conditions and the way the point in parameter space was approached.

Towards the boundary of the region of parameter space where a particular mode dominates the flow, the temporal and spatial structure of the flow generally became more complex. The simpler time dependent flow regimes observed are amplitude vacillation (AV) and structural vacillation (SV). For AV the amplitude of the wave varies periodically while the shape of the wave pattern remains constant. The strength of the vacillation is characterized by a *vacillation index*, I_{V}, as introduced by RBJS, and is defined over one vacillation cycle as

$$I_{\mathrm{V}} = \frac{A_{\max} - A_{\min}}{A_{\max} + A_{\min}}. \tag{3.1}$$

In an AV flow, I_{V} is a constant, but it varies over time if the vacillation itself is modulated. Amplitude vacillation of a zonal mode is found for values of Θ higher than those for the steady regime of the same mode. The transition from steady waves to AV is often a gradual one, and the distinction between them is somewhat arbitrary. A convention used by Hignett (1985) and RBJS chooses a critical vacillation index of $I_{\mathrm{V}} = 0.05$, below which the flow is said to be essentially steady. Large-amplitude

Table 3. *Experimental parameters and main frequencies of the experiments described in detail in the text*

(The labels are used in the text to refer to these experiments. $\mathcal{T}$, Θ, Gr are the Taylor number, the thermal Rossby number, and the Grashof number respectively. f_{d} and f_{v} are the drift and vacillation frequency of the dominant wave mode. $f_{m,i,a}$ in quasi-periodic flow is the frequency and in aperiodic flows the timescale of either the modulation, the bursting, or the wave number switching.)

label	regime	$\mathcal{T}$ $[\times 10^6]$	Θ	Gr $[\times 10^6]$	ω_{d}	ω_{v} $[\times 10^{-3}$ Hz]	$\omega_{m,i,a}$	
(a)	2+3IV	4.31	1.09	4.69	1.444	13.29	8.809	$\omega_{\mathrm{d}} = \omega_{\mathrm{d}2}, \omega_m = \omega_{\mathrm{d}3}$
(b)	2+3IV	3.85	1.09	4.21	1.282	12.76	8.301	$\omega_{\mathrm{d}} = \omega_{\mathrm{d}2}, \omega_m = \omega_{\mathrm{d}3}$
(c)	2SV	4.54	0.637	2.89	0.895	11.0	—	
(d)	3MAV	6.09	0.370	2.25	1.22	5.66	0.977	
(e)	3MAV	2.47	0.455	1.12	0.712	3.60	0.075	
(f)	3MAV	6.09	0.394	2.40	1.404	5.60	1.404	
(g)	3MAV-r	2.74	0.667	1.83	0.326	5.11	0.326	
(h)	3MAV-r	2.83	0.645	1.83	0.321	5.25	0.321	before locking
					0.329	5.25	0.329	after locking
(i)	3/2I	3.64	0.540	1.97	0.488	6.12	0.426	
(j)	3/2I	4.10	0.608	2.49	1.65	6.57	1.65	ω_i
							0.08	ω_m
(k)	2-3A	3.64	0.590	2.15	0.529	6.00	0.111	$\omega_{\mathrm{d}2}$, $\omega_{\mathrm{v}3}$, ω_a
(l)	3AV	3.64	0.527	1.92	—	6.41	—	stationary wave
(m)	3AV	3.85	0.526	2.03	—	6.47	$\omega_{\mathrm{v}}/2$	stationary wave

structural vacillation, on the other hand, occurs towards the geostrophic turbulence regime, i.e. at lower values of Θ and higher values of $\mathcal{T}$ than the respective steady wave. While the total wave amplitude, and with it the radial heat transport, remain fairly constant, the shape of the wave varies approximately periodically. Phase portraits of AV flows show quasi-periodic tori, but SV flow, of which a number of varieties have been observed, is generally less regular than AV, and phase portraits are not consistent with a simple torus. A weak structural vacillation, however, is observed for most of the 'steady' wave regime. This weak structural vacillation, which is identified with the 'wavering' of the 'jet' stream described by Hide (1953), is the subject of discussion of § 5.

The superposition of two steady waves with different zonal wave numbers and different phase speeds will result in a quasi-periodic oscillation of the flow field, termed an *interference vacillation* (IV). While interference vacillation has been previously observed in an annulus with a free surface (Pfeffer & Fowlis 1968), the present observation of the interference of two zonal modes, $m = 2$ and $m = 3$, is the first docu-

mented occurrence of interference vacillation in the thermal annulus with a rigid lid. The drift frequencies $\omega_{\mathrm{d}2}$ and $\omega_{\mathrm{d}3}$ were always found to be incommensurate, resulting in flow on a torus. The IV regime will be discussed in § 4.

In this study three main types of more complex flows were observed, one of which was a *modulated amplitude vacillation* (MAV), which involved zonal modes other than the dominant and its harmonics. The 3MAV was first investigated by RBJS and formed the motivation for this investigation. Two other complex flow types, which have not been reported before, consisted of (a) an intermittent distortion of the flow field by the growth of an $m = 2$ component at the expense of the basic 3MAV (3/2I), and (b) a flow type in which the flow alternated between two zonal wave modes, $m = 2$ and $m = 3$ (2-3A). These multi-mode states are the main focus of this paper and will be discussed in detail in § 6.

The flow denoted 'D' in figure 2, close to the lower axisymmetric regime, did not equilibrate to a pure regular wave state, but was characterized by irregular fluctuations of the first four azimuthal wave modes. These modes had amplitudes of about 2–3% of ΔT, compared to 5–8% for regular waves. Since the modes drifted independently through the annular channel without any apparent phase-locking, the regime is referred to as the *dispersive regime* (D). In more specific cases, subregimes of the dispersive regime are designated D_i with i denoting the zonal wave number which was on average the strongest. While the transition from the dispersive regime to the $m = 3$ regular waves was an abrupt one, at higher Θ the mode $m = 2$ gradually became more and more prominent, until the flow was either a marginally vacillating $m = 2$ or the interference vacillation 2+3IV. The drift frequency of wave 2 varied smoothly from the D_2 to the IV regime. Phase space reconstructions of D could not reveal any underlying structure in the irregular wave behaviour.

(*b*) *Pattern drift velocities*

It was noted that the drift velocity of the wave pattern showed some coherent behaviour independent of the dominant wave number; a trait which was observed by Hide (1958) in an annulus with a free surface. In figure 3 the drift speed of the dominant Fourier mode divided by the wave number is plotted for all experiments performed for this study. From the 2+3IV regime, both $\omega_{\mathrm{d}2}/2$ and $\omega_{\mathrm{d}3}/3$ are plotted. The majority of the points lie on a fairly well defined curve, denoted (A), with an appropriate functional form of

$$\omega_{\mathrm{d}}/m \propto Gr^{1.25\pm0.5}, \tag{3.2}$$

where m is the zonal wave number of the dominant mode and Gr the Grashof number, defined by

$$Gr = \mathcal{T}\,\Theta = 4g\alpha\,\Delta T\,L^3/\nu^2. \tag{3.3}$$

This not only confirms Hignett's (1985) observation that the phase speed was continuous across a wave number transition, but it also extends this relation to flows far from a wave number transition.

Apart from the cases following the 'regular' behaviour, there are two more distinct clusters, one at high phase speeds (B), and the other (C) branching off from the regular behaviour to very slow phase speeds. The branch C of rapidly decreasing ω_{d} (with increasing Gr) was formed by the 3MAV-r flows and those 2-3A flows which were close to the 3MAV-r regime. While the waves in all other experiments drifted with a positive (superrotating) phase velocity, these waves actually moved in

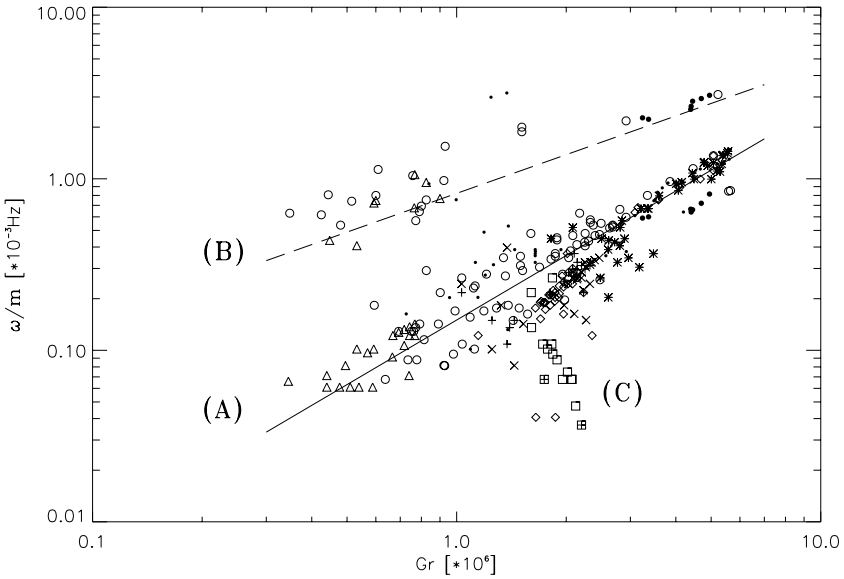

Figure 3. Phase speed of the dominant wave number *vs Gr* (see text and equation (3.3). The solid line (A) has a slope of 1.25, the broken line (B) has a slope of 0.75. The different symbols correspond to the following regimes: ○ 3 and 3MAV, □ 3MAV-r, ◇ 3/2I, + 2-3A ($\omega_{\mathrm{d}2}$), × 2-3A ($\omega_{\mathrm{d}3}$), ⋆ 2SV, △ 4MAV, • D and 2+3IV.

a retrograde sense around the annular channel. The drift period seemed to diverge towards the transition from the 3MAV-r to the 2SV flow with a longest observed drift period of $\tau_{\mathrm{d}} \approx 7000$ s. The change in the phase speed seemed to follow a functional dependence on the distance from a critical value of $\mathcal{T}$ as

$$\omega_{\mathrm{d}} \propto -\mu^{0.65\pm0.05}, \tag{3.4}$$

where $\mu \equiv \mathcal{T}_c - \mathcal{T}$ with $\mathcal{T}_c = (3.6 \pm 0.1) \times 10^6$. The given standard deviation in the exponent is obtained as a formal error from the regression analysis, but does not include any effect of the uncertainty in the value of $\mathcal{T}_c$. With this uncertainty included, the uncertainty in the exponent is estimated at around ± 0.2. Since this phenomenon was only observed for a very small range of Θ, this regression could not capture any possible dependence on Θ or combinations of $\mathcal{T}$ and Θ.

The experiments which cluster around branch B at fairly high values of ω_{d}, were found either to be long-lived transients or the $m = 3$ mode in the 2+3IV regime. When the apparatus was spun up from rest, initial transients would normally decay after $O(10\,\mathrm{min})$. After this the flow could settle either into equilibrated flow with ω_{d} on branch A, or into a metastable transient AV with a very high phase speed. The range of drift frequencies observed for the transient AV was between 10^{-3} and 10^{-2} Hz, generally a factor *ca.* 5 faster than for the finally equilibrated flow. Occasionally the drift frequency was observed to be identical to the vacillation frequency. These transients had a variable life time, but they could persist for up to 30 h before undergoing the final transition to waves with drift frequencies on the main branch A. The transition from the fast transient AV to the equilibrated flow took $O(10\,\mathrm{min})$, and, compared to the transient, the time averaged spatial wave spectrum showed increased intensity in the sidebands after the transition.

4. Interference vacillation

The flow designated as interference vacillation (2+3IV) can be described as the superposition of two waves. While this coexistence of two zonal modes has been observed in annulus experiments with a free surface by Pfeffer & Fowlis (1968) and Kaiser (1970), no occurrence of interference vacillation has been previously reported in an annulus with a rigid lid. In our case, waves $m = 2$ and $m = 3$ travelled with different phase velocities through the annulus, while vacillating weakly and apparently irregularly with a rather high frequency of $O(0.04\,\mathrm{Hz})$. The pattern drift frequency ratio observed in our experiments ranged from $\omega_{\mathrm{d}3}/\omega_{\mathrm{d}2} = 5.56$ to 8.16 without any indication of frequency locking between the two drift frequencies. Of the two modes the mode $m = 2$ followed the scaling of equation (3.2) with $\omega_{\mathrm{d}2} = O(10^{-3}\,\mathrm{Hz})$, but $m = 3$, which would normally be expected to have a drift frequency around $3/2\omega_{\mathrm{d}2}$, travelled at a much higher frequency of $\omega_{\mathrm{d}3} = O(7 \times 10^{-3}\,\mathrm{Hz})$ corresponding to branch B in figure 3. Despite the vacillation—at first sight a third frequency—the phase portrait was for most of the IV regime a clean T^2-torus, indicating that the vacillation was linked to the two drift frequencies. Towards lower Θ, a somewhat slower vacillation became apparent in conjunction with the break-up of the T^2-torus to a more complex and irregular 'fuzzy' torus.

Theoretical studies of two-layer models (Hart 1981; Pedlosky 1981) have shown that no mixed wave states would be stable on an f-plane. Including the β-effect introduces dispersion into the system, and the bifurcation analysis by Moroz & Holmes (1984) of a weakly nonlinear two-layer model produced stable mixed-wave states, but only for adjacent wave numbers above $m = 4$. For the other wave numbers, the mixed-wave states were found to be unstable, showing a hysteretic wave number transition instead. Mansbridge (1984), also using a two-layer model, studied the effect of varying β on wave number transitions and found that adjacent wave numbers could coexist above a critical value for β/r, where $r = \sqrt{\nu f}/U = \sqrt{E}/Ro$ is the Ekman-dissipation parameter generally used in two-layer models. The critical value for β/r varied from 102 for $m = 1$ and 2, with a minimum of 43 for $m = 5$ and 6, rising back to $(\beta/r)_{\mathrm{crit}} = 63$ for $m = 9$ and 10.

The apparatus of the present study had flat end walls, and thus the flow was to first order on an f-plane. Hide & Mason (1978) argued, however, that in this apparatus the basic axisymmetric flow has a non-zero radial potential vorticity gradient due to the vertical variation of the horizontal flow. From numerical simulations of axisymmetric flow they calculated a potential vorticity gradient comparable to U/L^2. Using this for β^*, with $U = 10^{-2}\mathrm{m\,s^{-1}}$ and the other quantities from table 1, we obtain $\beta/r = \beta^* LD/\sqrt{2\nu f} = 0.7$, well below the critical values found by Mansbridge (1984).

In a linear superposition of two steady modes the zonal flow component would be steady as well. Ohlsen & Hart (1989*a*), however, observed a form of nonlinear interference vacillation of the zonal modes $m_1 = 1$ and $m_2 = 2$ in a mechanically forced two-layer system which resulted in an oscillation of the zonal flow component at a frequency $\omega_0 = 2\omega_1 - \omega_2$. They argued in another paper (Ohlsen & Hart 1989*b*) that a zonal flow component with the frequency $\omega = |m_1\omega_2 - m_2\omega_1|$ could be forced through a chain of triad and self interactions. This interaction scenario, applied to our case of $m_1 = 2$ and $m = 3$, is shown in figure 4*a*. The chain would comprise the triad (2|3|1) transferring energy into $m = 1$ with $\omega_1 = \omega_{\mathrm{d}3} - \omega_{\mathrm{d}2}$. Mode $m = 1$ then could force its harmonic through self interaction, $1 \rightarrow 2$, with $\omega_2 = 2\omega_{\mathrm{d}3} - 2\omega_{\mathrm{d}2}$. The resulting $m = 2$ would finally interact with the original $m = 2$ to give a zonal

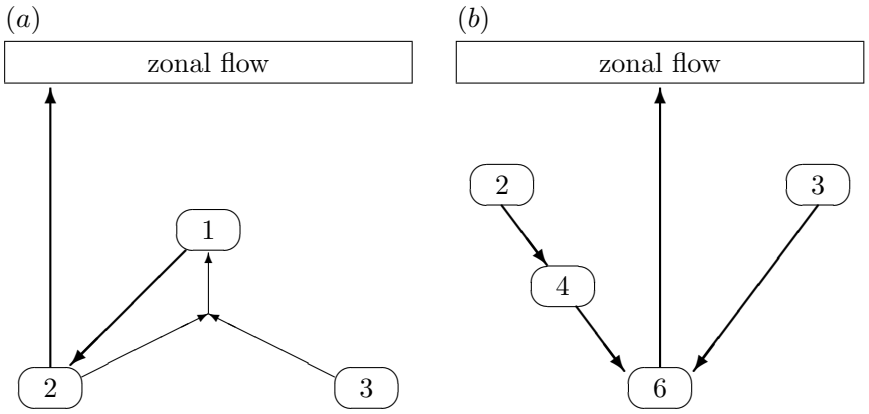

Figure 4. Wave interaction mechanisms for nonlinear interference vacillation, (*a*) following Ohlsen & Hart (1989*b*), and (*b*) the mechanism observed in these experiments.

flow correction with $\omega = |3\omega_{\mathrm{d}2} - 2\omega_{\mathrm{d}3}|$. In Ohlsen & Hart's experiments, however, in which modes $m = 1$ and 2 were dominant, the interactions are somewhat degenerate because one of the dominant modes is also the harmonic of the other, and the other is the long wave itself.

Analysis of the vacillation frequency in our quasi-periodic IV regime showed indeed that $\omega_{\mathrm{v}} = 2\omega_{\mathrm{d}3} - 3\omega_{\mathrm{d}2}$. It was observed, however, that the modes $m = 4, 5, 6$ showed much stronger peaks in their power spectra than the long wave. Also, triads involving the modes $m \geqslant 2$ showed stronger phase locking than triads including the long wave, $m = 1$, as measured by the maximum value and half-width of the triad locking probability density function defined in equation (A 4). As shown in figure 5 the long wave triad (3|2|1) has a rather low and broad maximum of $\rho_{3-2-1} = 0.4$ at $\varphi = \pi$, whereas the harmonic triad has a well defined peak of $\rho_{6-4-2} = 0.9$ at $\varphi = \pi/2$.

With modes $m = 2$ and $m = 3$ it is also possible to produce a zonal flow oscillation with the observed frequency by harmonic and self interactions only, because $m = 6$ is a harmonic of both dominant modes, as shown in figure 4*b*. Thus $m = 2$ would force $m = 6$ with $\omega = 3\omega_{\mathrm{d}2}$, and $m = 3$ would force it with $\omega = 2\omega_{\mathrm{d}3}$. This interaction scenario is possible for all pairs of adjacent zonal wave numbers $\{m, m+1\}$ since the mode $m' = m \times (m+1)$ is forced by m with frequency $(m+1)\omega_m$ and by mode $m+1$ with frequency $m\omega_{m+1}$ resulting in a zonal flow correction with the frequency $|(m+1)\omega_m - m\omega_{m+1}|$.

Towards lower Θ, where the torus was unstable, no similar relationship between the wave drifts and the vacillation could be detected, and also the phase locking was different from the quasi-periodic IV. While most triads were largely unaffected, the preferred phase relation of the harmonic triad changed from $\varphi_{6-4-2} = \pi/2$ to $5\pi/4$. Close to the transition to the D_2 regime the quasi-periodic IV underwent a torus-doubling bifurcation as illustrated by the return maps in figure 6. The simple torus (case (a)) in figure 6*a* has doubled in the transition to case (b), shown in figure 6*b*, with the 8-shaped first return map which becomes a circle in the second return map. It appears that the transition to the irregular D_2 is possibly through only one torus-doubling bifurcation followed by another torus instability. The nonlinear interactions in the harmonic triad seem to be an essential feature in stabilizing the nonlinear interference vacillation.

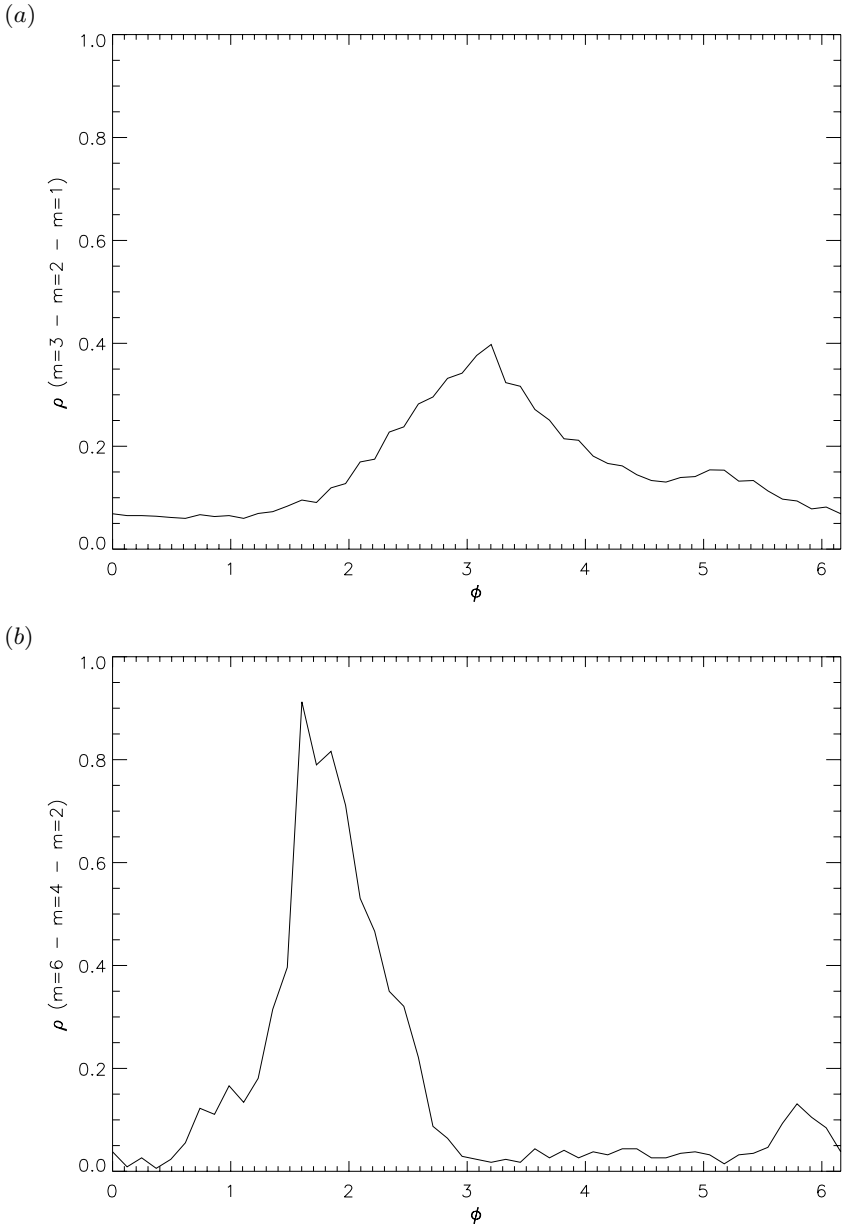

Figure 5. IV regime, case (a): triad locking probability density function for the triads (*a*) (3|2|1), and (*b*) (6|4|2).

5. Weak structural vacillation (2SV)

At values of $\mathcal{T}$ and Θ greater than those for the $m = 3$ flows, a weak structural vacillation of an $m = 2$ flow was observed (see regime diagram in figure 2). The occurrence of vacillation at this range of parameters was initially surprising, since RBJS had reported a marginally steady wave in this region of parameter space only showing the barely perceptible wavering of the jet stream of steady wave patterns

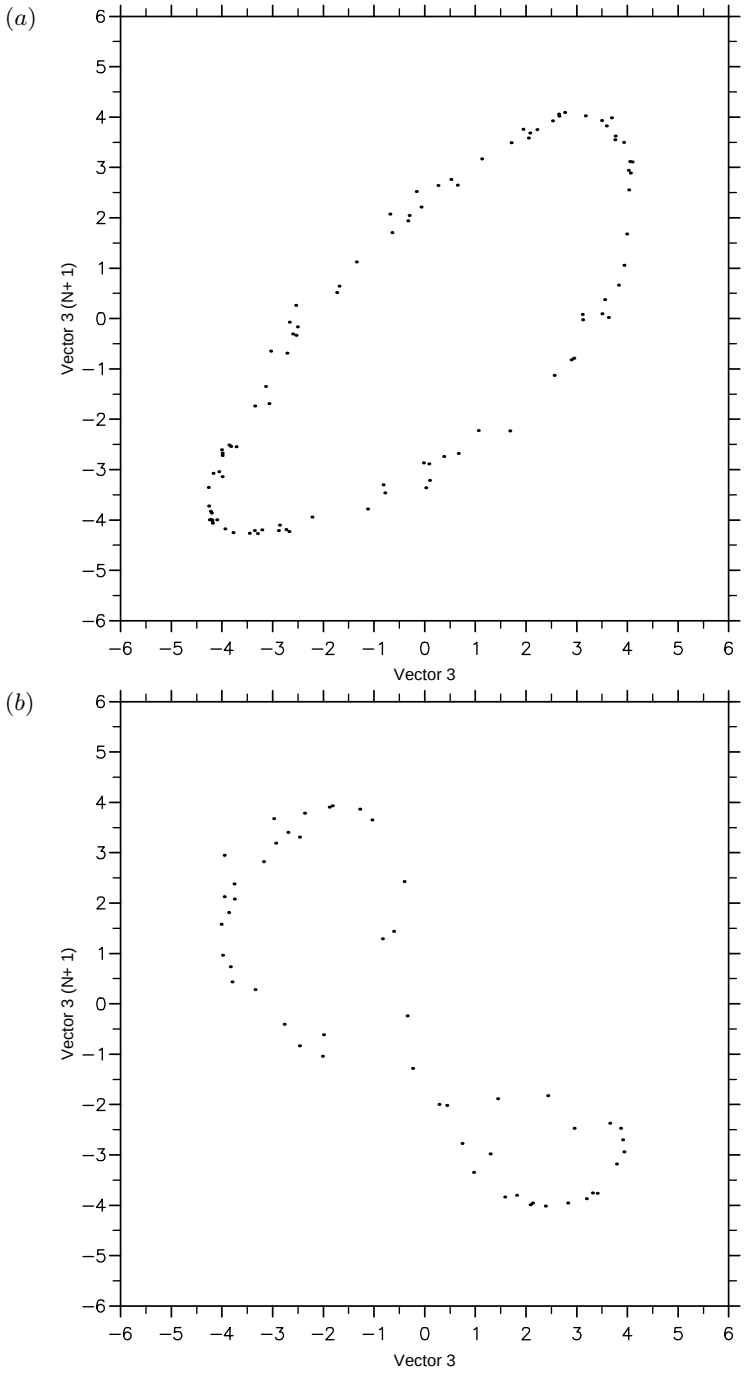

Figure 6. IV regime: return map of Poincaré sections at vector $1 = 0$; (*a*) for case (a) in the centre of the regime, and (*b*) for case (b) close to the transition to the D_2 regime.

(Hide 1953). It is, however, unlikely that a steady and a vacillating flow of the *same* wave number could co-exist.

The weak vacillation seemed to be related neither to the observed amplitude vac-

illation nor to the structural vacillation reported by RBJS; the vacillation frequency was not similar to the vacillation frequency of the AV flows, and the phase space reconstruction was entirely different from the phase portraits obtained for SV by RBJS. It is more likely that the actual regimes of RBJS and the present study are identical, and that the apparent discrepancy is an artefact of the thermocouple arrangements.

A possible explanation may be found by comparing two cases from our experiments at similar parameter values, one of which used the double thermocouple ring measuring at $y = (r - a)/(b - a)$ of 1/4 and 3/4 respectively, while the other employed the single thermocouple ring with the thermocouple junctions at $y = 1/2$ as used by RBJS. The experiment measuring at mid-radius gave as the vacillation index (cf. equation (3.1)) $I_{\mathrm{V}} = 0.04$ and would be classified as a steady wave 2, following Hignett (1985). Measuring at $y = 1/4$, however, resulted in $I_{\mathrm{V}} = 0.13$, and at $y = 3/4$ even $I_{\mathrm{V}} = 0.31$. Furthermore, comparing the wave amplitude at the inner thermocouple ring with that at the outer ring revealed that their vacillations were in antiphase: an amplitude maximum at the outer ring coincided with a minimum at the inner ring. This suggests that the wave can be kinematically described by the superposition of a steady gravest radial wave mode ($m = 2$, $n = 1$) and a small amplitude oscillation of the second radial mode ($m = 2$, $n = 2$). This description of SV is consistent with observations by Pfeffer *et al.* (1980), who used a three-dimensional array of 2016 thermistors in a free-surface annulus. Weng *et al.* (1986) found a quasi-periodic structural vacillation in a numerical model of a continuously stratified fluid, which contained two different radial modes of the same zonal wave number. Their structural vacillation was characterized by an almost steady first radial mode, superimposed on which was an oscillatory second radial mode. Consistent with our observations, the mean amplitude and strength of the vacillation of the second radial mode was considerably weaker than the amplitude of the steady gravest radial mode. As in our observations, their vacillation frequency was also higher than a typical AV vacillation frequency. The second radial mode has a node near the channel centre, and thus is not easily detected by probes at mid-radius. The time series in figure 7*a*, which shows the vacillating amplitudes of the azimuthal wave at the inner and outer thermocouple ring, respectively illustrates the phase shift between the two vacillations.

The power spectrum of the temperature time series has distinct peaks at the drift and vacillation frequencies (labelled ω_{d} and ω_{v} in figure 7*b* with $\omega_{\mathrm{d}} = 9 \times 10^{-4}$ Hz and $\omega_{\mathrm{v}} = 1.1 \times 10^{-2}$ Hz), together with higher harmonics, and their sum and difference components. This suggests well defined dynamics governing both the large-amplitude drifting wave and the relatively weak vacillation, and one would expect flow on a torus. The phase portrait, however, only reveals a thickened limit cycle (figure 8*a*);† the Poincaré section, too, could not reveal any further structure. Instead of observing a—possibly noisy—toroidal surface, the trajectory appears to cover the entire interior of the torus (figure 8*b*). The large scale structure of the drifting wave pattern is very well represented by a limit cycle but the vacillation with a distinct frequency of $\omega_{\mathrm{v}} \approx 10^{-2}$ Hz in the power spectrum could not be captured by a low-dimensional phase space reconstruction. Consequently the Grassberger–Procaccia algorithm (Grassberger & Procaccia 1983), failed to give consistent scaling.

† To enhance the clarity of three-dimensional phase portraits, the trajectory is broadened into a ribbon, where the orientation of the ribbon is determined by the curvature of the trajectory, as described by Darbyshire & Price (1990).

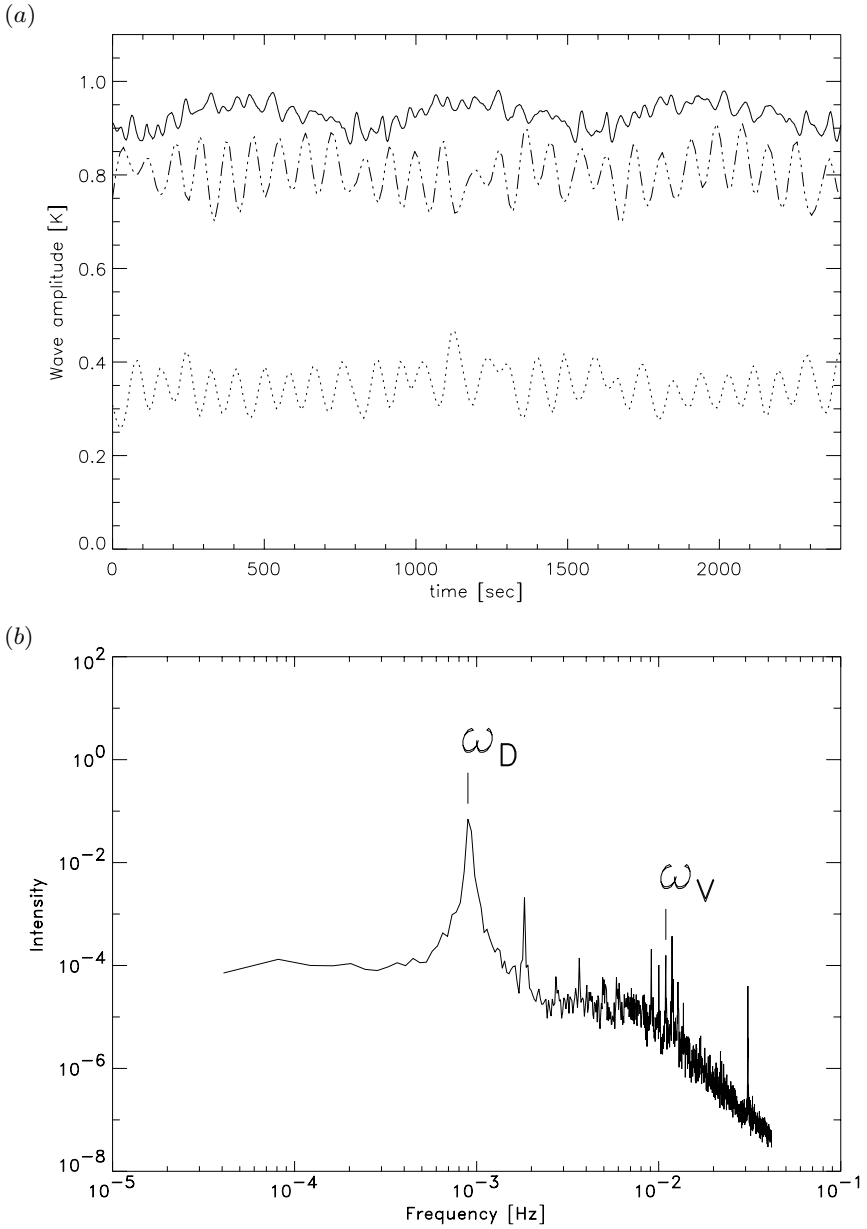

Figure 7. 2SV regime: (*a*) superposition of time series of wave amplitudes of modes $m = 2$ from two experiments: the dash-dotted line is from case (c) at $y = 1/4$, the dotted line from case (c) at $y = 3/4$, and the solid line is from an experiment measuring at $y = 1/2$. (*b*) Power spectrum of the thermocouple temperature at $y = 1/4$ from case (c).

The correlation integral, given in figure 8*c*, shows two distinct regions, a small scaling region at large phase space radii with a small correlation dimension of around $d_c = 1.3$, corresponding to the limit cycle structure of the steady first radial mode, and a region where the correlation integral falls off rapidly, possibly converging to an attractor dimension of $d_c \approx 4.5$. The total heat flux in figure 8*d* only shows a high

slope with $d_c \approx 5.8$. This behaviour has also been reported by Guckenheimer & Buzyna (1983) for temperature measurements of the fluid interior in a thermally driven rotating annulus. While for amplitude vacillation they found clear scaling regions with slopes around $d_c \approx 3$, their analysis of structural vacillation showed two scaling regions. For larger values of the phase space radius the correlation integral had a slope of $d_c = 1.6$, which as the radius was decreased gave way to a slope around $d_c \approx 7$. Similarly, RBJS observed for 3SV that the dimension estimates for time series of the fluid temperature and the total heat flux were not consistent with each other.

The existence of a distinct frequency of the apparently irregular vacillation suggests a secondary dynamic instability of the flow, which RBJS suggested is manifest as spatially localized transients and thus cannot be described by global dynamics represented in phase space reconstructions. As mentioned above, the high-dimensional nature of the observed SV is consistent with SV flows observed in other investigations, but structural vacillations of baroclinic waves are much more diverse than amplitude vacillations. Tamaki & Ukaji (1993), for instance, observed a quasi-periodic—and thus low-dimensional—form of structural vacillation in a thermally driven rotating annulus with a free surface, which was also found in numerical integrations (Ukaji & Tamaki 1990). In contrast to the SV observed in this study, the time series of the amplitude of the dominant zonal wave mode at an inner and an outer location was mainly in phase, with the wave amplitude at mid-radius vacillating out of phase with these.

6. Flows dominated by $m = 3$

At very low values of Θ, $\Theta \lesssim 0.1$, depending on the initial conditions, the flow either equilibrated to a steady $m = 3$ or to a complex $m = 4$ MAV state. Over most of the $m = 3$ region, however, the amplitude of the $m = 3$ Fourier component varied over time, either in the form of a periodic oscillation (AV) or a more complex modulated oscillation, such as the MAV. The only highly regular quasi-periodic AV observed was the small 3AV regime observed at large values of Θ ($\geqslant 1.0$); all apparent 3AV flows observed at smaller values of Θ were interspersed among multi-mode 3MAV flows, and they were found to be frequency-locked states (see below, § 6 *b*). The amplitude of the vacillation, as measured by the vacillation index I_{V} (equation (3.1)), increased with Θ throughout the main $m = 3$ region from $I_{\mathrm{V}} \approx 0.05$ around $\Theta = 0.1$ to $I_{\mathrm{V}} = 0.85$ for the 3MAV-r flow at $\Theta = 0.8$. The isolated 3AV region at even larger values of Θ, however, had a smaller value for I_{V} of *ca.* 0.75. The gradual increase of I_{V} with Θ was also observed by Fowlis & Pfeffer (1969) in a larger annulus (with a free-surface), and by Hignett (1985) in an annulus identical to the present but with a fluid of smaller Prandtl number $Pr \approx 13$. Studies of the effect of Pr on the vacillation by Jonas (1981) and Pfeffer *et al.* (1980) noted that at higher Prandtl numbers, vacillating waves became more widespread at the expense of the steady wave regime. The increased stability of steady waves in fluids with lower viscosities shows that the equilibration of the baroclinic flow to steady wave patterns is not merely a product of viscous effects, but must be explained by nonlinear feedback mechanisms. Hignett (1985) reported observing extended regions of steady waves in a fluid with $Pr = 13$, though these were classified with a thermocouple ring at $y = 1/2$ and thus might be either steady waves or a weak structural vacillation.

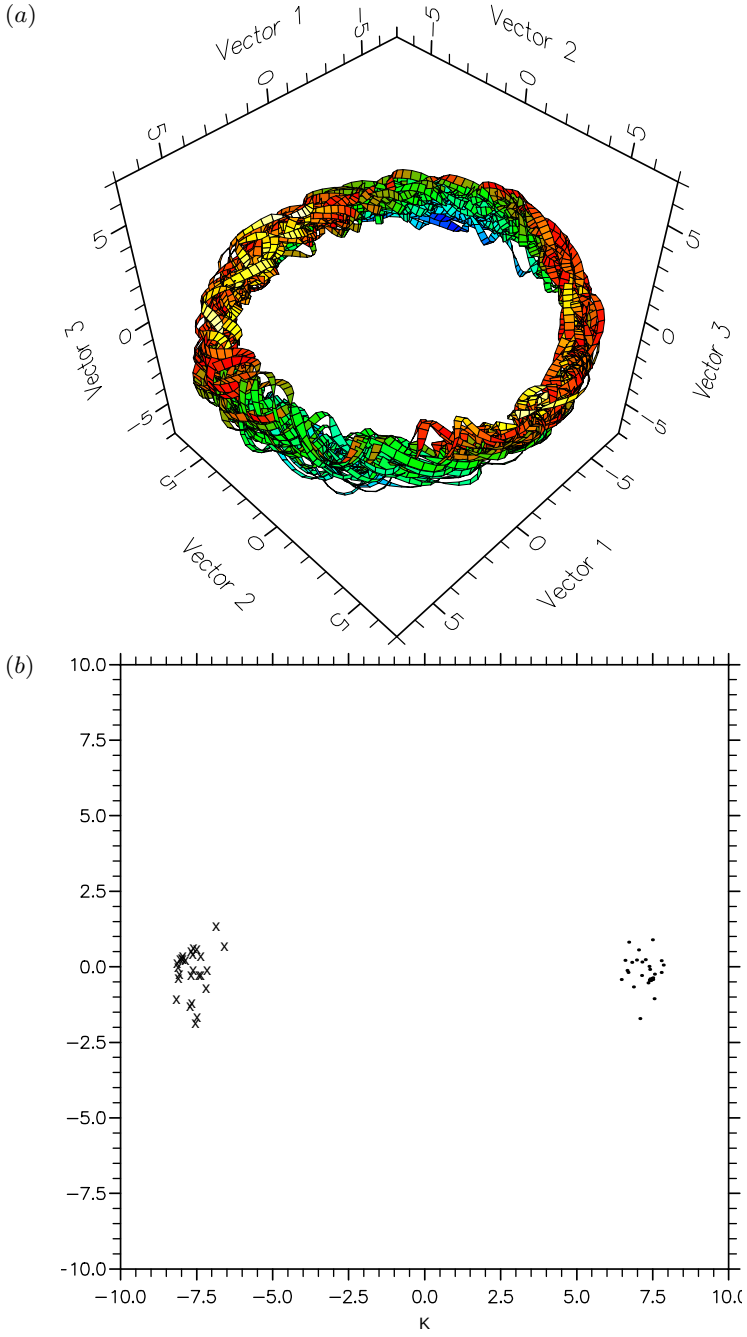

Figure 8. 2SV regime, case (c): (*a*) phase portrait, (*b*) Poincaré section at vector 1 = 0.

Using an identical apparatus, and a higher $-Pr$ fluid, RBJS and the present study found only flows which marginally satisfied the criterion for steady flow (cf. equation (3.1)) with $I_{\mathrm{V}} \approx 0.05$. These almost steady wave flows, found at $\Theta \leqslant 0.1$, still showed distinct peaks at the vacillation frequency in the power spectrum of the temperature data.

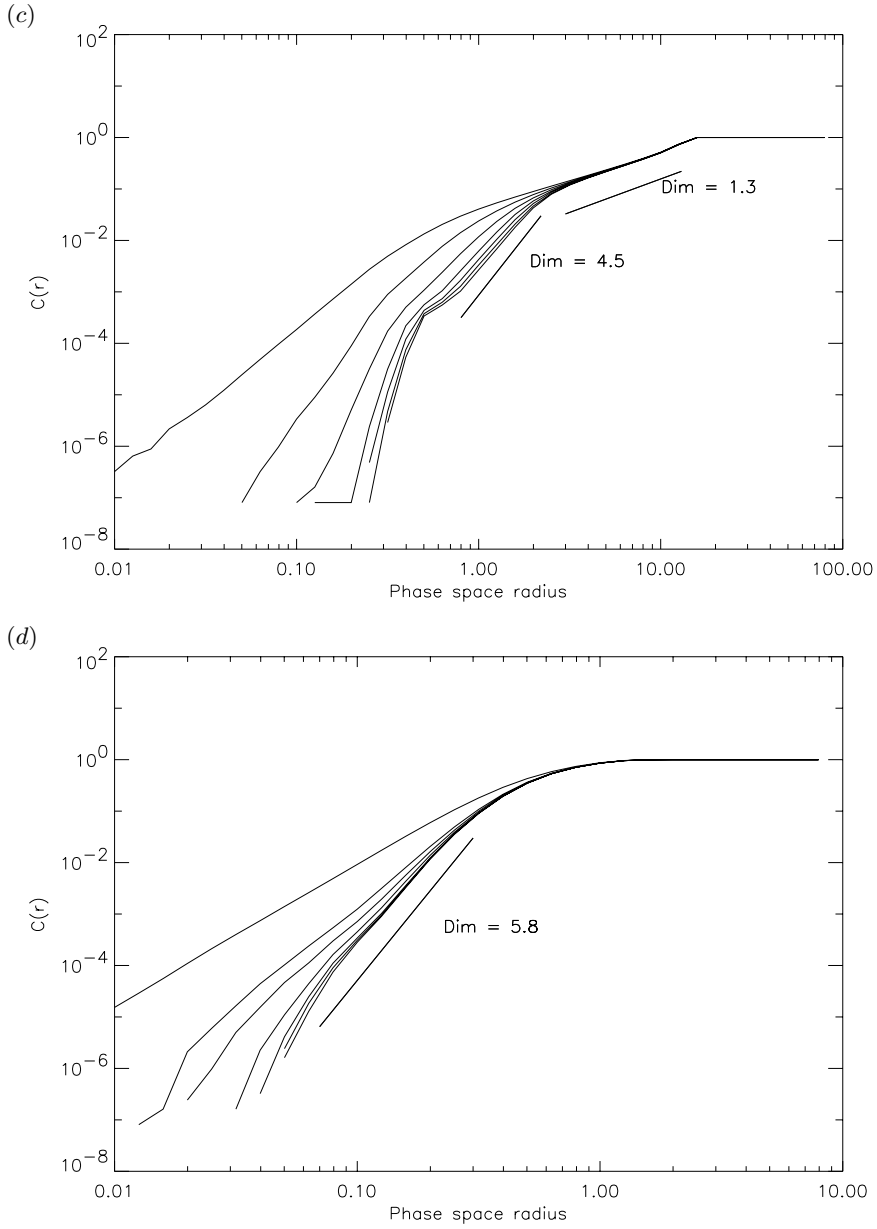

Figure 8. *Cont.* Correlation integral for reconstructed phase portrait: (*c*) thermocouple ring data, (*d*) heat flux.

The vacillation frequency, $\omega_{\mathrm{v}3}$, seemed largely independent of Θ throughout the time-dependent $m = 3$ flow regimes, but increased with $\mathcal{T}$ (see figure 9*a*):

$$\omega_{\mathrm{v}3} \propto \mathcal{T}^{0.6\pm0.1}. \tag{6.1}$$

The data were obtained from all AV, MAV and 3/2I flows of this study. The scaling of the vacillation frequency is in very good agreement with the findings by RBJS who observed a scaling of $\omega_{\mathrm{v}3} \propto \mathcal{T}^{0.62}$. The present experiments resulted in scaling

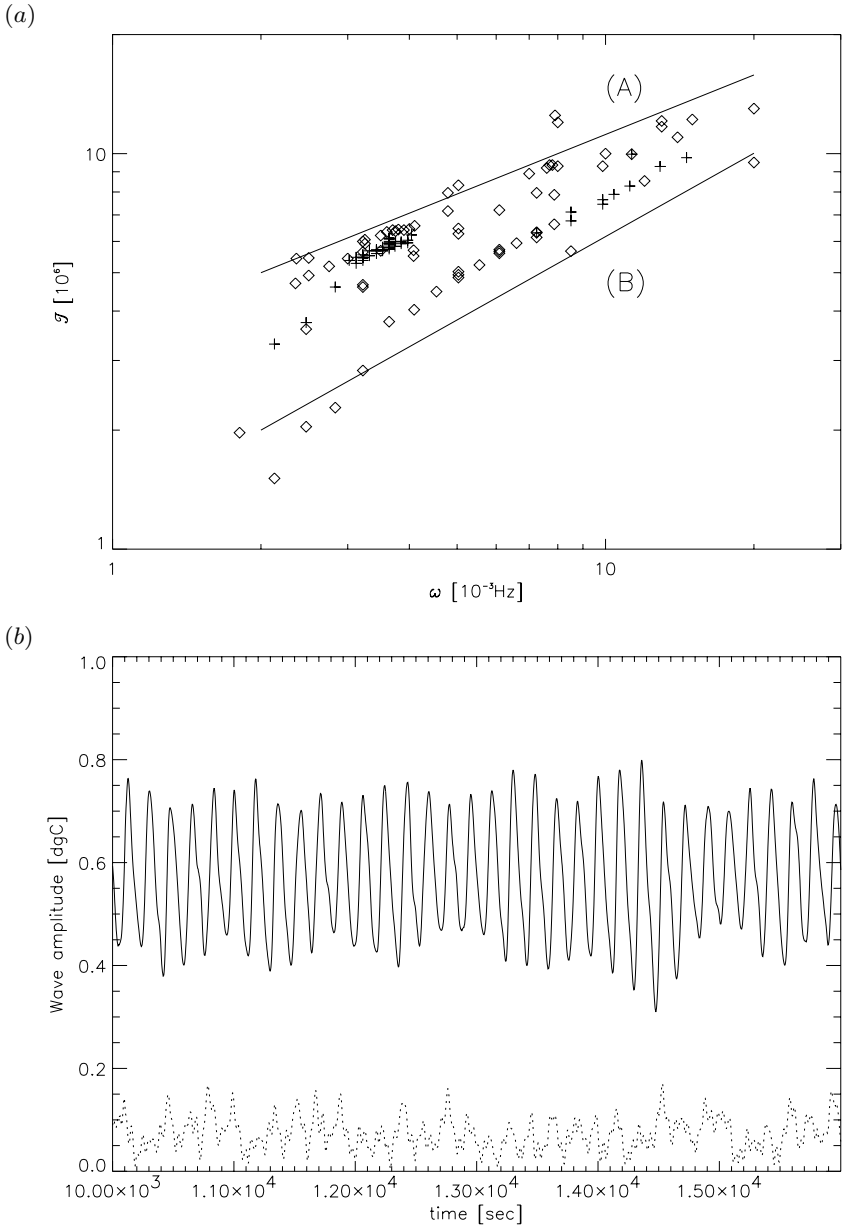

Figure 9. 3MAV regime: (*a*) scaling of the vacillation frequency of the $m = 3$ wave mode with $\mathcal{T}$. Curve (A) has a slope of 0.5, and curve (B) a slope of 0.7. (*b*) Time series of wave amplitudes of azimuthal wave modes $m = 3$ (solid line) and $m = 2$ (dashed line) from case (d).

exponents ranging from 0.4 to 0.7, where some sets of experiments showed scaling very close to $\omega_{\mathrm{v}} \propto \sqrt{\mathcal{T}}$ (in this case the vacillation frequency would be a linear function of the background rotation). The vacillation frequency in the 3MAV-r flow might also be consistent with the scaling in equation (6.1) with $\omega_{\mathrm{v}3} \propto \mathcal{T}^{0.67}$, but it might on the other hand be determined by the specific scaling of the drift and modulation frequencies of this regime with $\omega_{\mathrm{d},m} \propto -(\mathcal{T}_c - \mathcal{T})^{0.65}$ (cf. equation (3.4)).

If both frequencies showed the same scaling exponent of 0.65, say, then their ratio would scale as $\omega_{\mathrm{d},m}/\omega_{\mathrm{v}} \propto -(\mathcal{T}_c/\mathcal{T}-1)^{0.65}$.

(*a*) *Modulated amplitude vacillation*

The strength of the vacillation was frequently observed to be weakly modulated on timescales of the order of the drift period or longer, where the modulation of the $m = 3$ mode was usually linked to a modulation of the weaker zonal modes. This modulated amplitude vacillation regime was studied in detail by RBJS. In this regard our experiments were a continuation of their study, addressing the role of nonlinear interactions, especially resonant triad interactions and frequency locking. The 3/2I flow which, strictly speaking, is a form of MAV, and which gradually evolves from the simple 3MAV upon change of parameters, is discussed separately below. Apart from this, two types of modulated amplitude vacillation were observed in this study, denoted respectively as 3MAV and 3MAV-r.

A fairly typical example of a 3MAV flow (case d) is given in figure 9*b*, which shows a time series of the wave amplitudes of $m = 3$ and $m = 2$ from the spatial Fourier analysis of the temperature data. The vacillation of the amplitude of wave 3 with a period of *ca.* 177 s $\approx 62\tau_0$ can be seen, where τ_0 is the rotation period of the apparatus, superimposed on which is a modulation of the amplitude on a timescale of *ca.* 1000 s $\approx 355\tau_0$. Decreases in the intensity of the amplitude vacillation of $m = 3$ are associated with increased activity in wave 2. The wave 3 pattern drifts along the annular channel with a period of *ca.* 820 s $\approx 287\tau_0$ without any indication of locking between these three frequencies.

The regime denoted 3MAV-r showed a much stronger vacillation index and a rather unusual wave propagation. Unlike all other flows observed, the dominant mode drifted slowly through the channel in a retrograde direction, opposite to the background rotation. While the vacillation frequency was consistent with the other 3MAV and 3AV flows, the drift frequency seemed to tend to zero close to the transition to the 2SV regime, following the scaling given in equation (3.4) (branch C in figure 3).

(*b*) *Frequency entrainment*

Due to the common occurrence of frequency locking of ω_m to ω_{d}, no clear relation between the experimental parameters and the modulation frequency could be detected. The lowest frequencies, however, were observed for small values of the Grashof number (case e with $\omega_m = 7.5 \times 10^{-5}$ Hz at $Gr = 1.12 \times 10^6$). This observation is consistent with the experiments by RBJS, though the extent of the MAV regime in the present study was larger than reported by RBJS, extending to smaller values of both $\mathcal{T}$ and Θ. An exception to the rule of ω_m increasing with Gr was the observed modulation of the 3MAV-r flow, in which ω_m was always found to be equal to ω_{d}, and therefore decreasing with increasing $\mathcal{T}$.

Locking of the vacillation frequency to any of the other frequencies was much less common. Entrainment of ω_{v} by ω_{d}, but not by ω_m or vice versa, was never observed, but a few isolated cases were observed in which all three frequencies were locked or almost locked. In those cases the generic three-frequency flow collapsed onto a periodic limit cycle. Ratios observed in the 3MAV regime included $\omega_{\mathrm{v}}/\omega_{\mathrm{d},m} = 5$ and 3, and occasionally the flow was a pure 3AV which could be interpreted as locking of ω_m to $\omega_m = \omega_{\mathrm{v}}$. In one case (f) the locking was incomplete, or intermittent, in that for a while the frequencies were in a ratio of $\omega_{\mathrm{v}}/\omega_{\mathrm{d}} = 4$ followed by a rapid phase shift before the frequencies again took this integer ratio. Furthermore, the

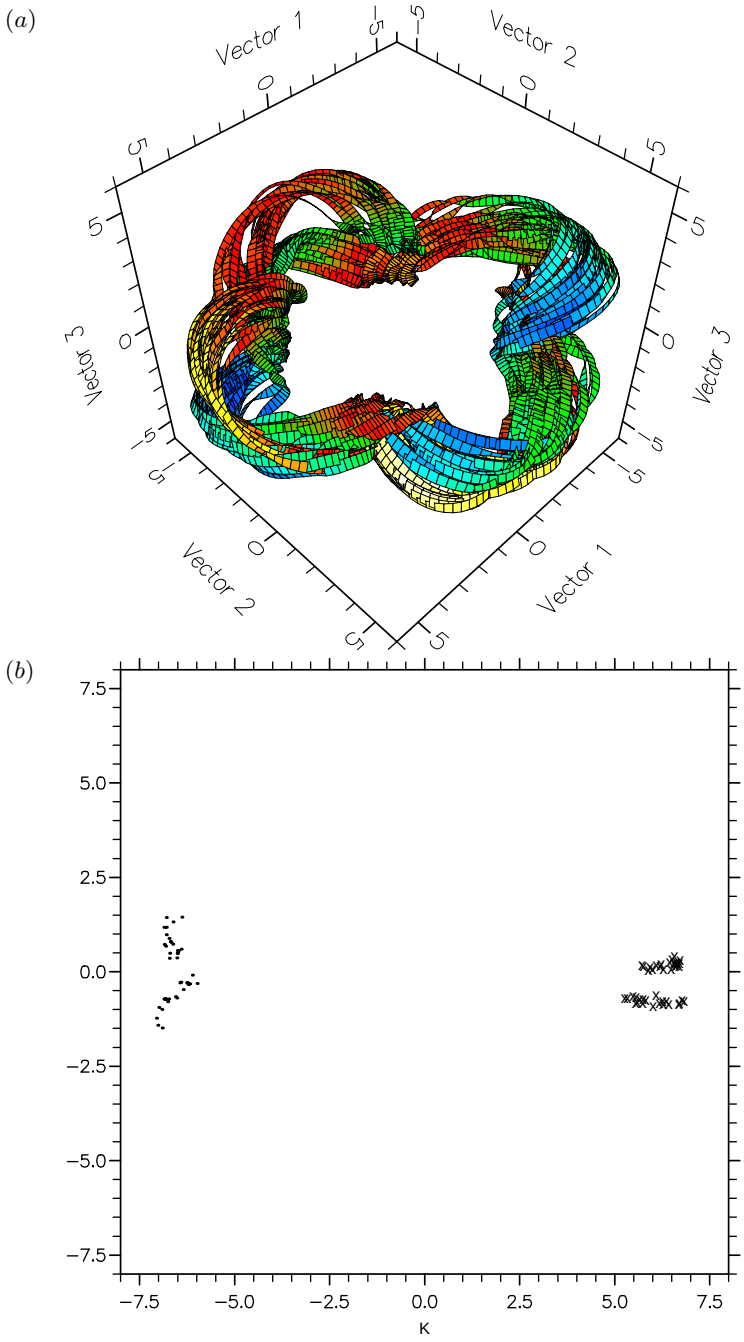

Figure 10. 3MAV regime, case (f): (*a*) phase portrait, and (*b*) Poincaré section at vector 1 = 0 of fully frequency locked flow.

incompletely locked oscillation was period-doubled, but instead of a period-doubled limit-cycle the trajectory was stretched into a period-doubled 'ribbon'. This is shown in the phase portrait and the Poincaré section in figure 10.

An example of the very long timescale sometimes associated with the onset of

frequency entrainment by the vacillation was found in the 3MAV-r regime. While for all observed flows in this regime the modulation frequency was locked to the wave drift with $\omega_m = \omega_\mathrm{d}$, the vacillation frequency was generally incommensurate to the drift frequency, ranging from $\omega_\mathrm{v} = 6.3\omega_\mathrm{d}$ to $41.7\omega_\mathrm{d}$ over the investigated 3MAV-r regime. This was reflected in the toroidal structure of the attractor in phase space reconstructions. In one experiment (case h), however, it was observed that the modulation suddenly became more pronounced after *ca.* $4000\tau_0$. Phase space reconstructions, carried out separately over the two halves of the time series, offered an explanation for this change: while before the transition the trajectory filled the surface of a torus, the orbit after the transition clustered around a limit cycle with a frequency ratio of $\omega_\mathrm{v} = 16\omega_\mathrm{d}$ (see figure 11). At the transition the drift frequency changed from $\omega_\mathrm{d} = 3.21 \times 10^{-4}$ Hz to 3.29×10^{-4} Hz—a change of 2.6%—while the vacillation frequency remained unchanged.

In the 4MAV regime the coupling of the vacillation frequency to the other two frequencies, ω_d and ω_m, appeared to be much stronger than in the 3MAV regime. Not only was the modulation frequency always found to be equal to the drift frequency, but also the drift frequency was always found to take an integer ratio of either $\omega_\mathrm{v}/\omega_{\mathrm{d},m} = 4$ or occasionally $\omega_\mathrm{v}/\omega_{\mathrm{d},m} = 3$.

(*c*) *Mode interaction*

Hide *et al.* (1977) and RBJS reported a strong phase coherence of the dominant mode with its sidebands, as measured by the sideband phase locking function $\Phi_m = 2\phi_m - \phi_{m-1} - \phi_{m+1}$ defined in equation (2.5). Hide *et al.* (1977) suggested the significance of a sideband instability akin to the Benjamin–Feir instability (Benjamin & Feir 1967), in which the dominant mode transfers energy to its sidebands with a long-wave modulation of the flow. In the case of the annulus with its discrete wave spectrum, the long-wave is the zonal mode $m = 1$. This mechanism, shown schematically in figure 12*a*, was supported by a theoretical study of small-amplitude Rossby waves in a channel (Plumb 1977), which showed that such a wave may be unstable to sideband interactions. A wave with the total horizontal wave number (m, n) and wave vector $\boldsymbol{k} = (k, l)$ ($k = 2\pi m/\alpha$ and $l = \pi n$ with α the channel aspect ratio) is unstable to weak sideband interactions if $k/l < 0.681$, and unstable to stronger triad interactions otherwise. If the results from small-amplitude Rossby waves in a straight infinite channel carry over to the large-amplitude waves in the annulus, then with $(m, n) = (3, 1)$ and $\alpha \approx 6$ the condition would not be satisfied with $k/l \approx 1$. Taking into account the side wall boundary layers and the curvature of the channel, the effective aspect ratio will be larger than 6. With an effective aspect ratio of $\alpha = 9$ the criterion would be met with $k/l = 0.67$. Thus the observed wave satisfied conditions close to where the theoretically preferred mechanism changes from the sideband interaction to triad interactions.

A different mechanism to explain the sideband phase locking, shown in figure 12*b*, was proposed by James *et al.* (1981) based on observations from numerical simulations of a steady wave. They found that the primary energy source for the sidebands was the first harmonic of the dominant mode, forming a triad $(2m|m - 1|m + 1)$. Both mechanisms would result in sideband phase locking with a minimum net forcing of the sidebands at $\Phi_m = \pi$. To distinguish these two mechanisms it is suggested here to analyse the phase coherence of wave triads with the triad locking probability density function as defined in equation (A 4). The long-wave mechanism can be regarded as the coupling of two *almost* resonant triads $(m|m - 1|1)$ and

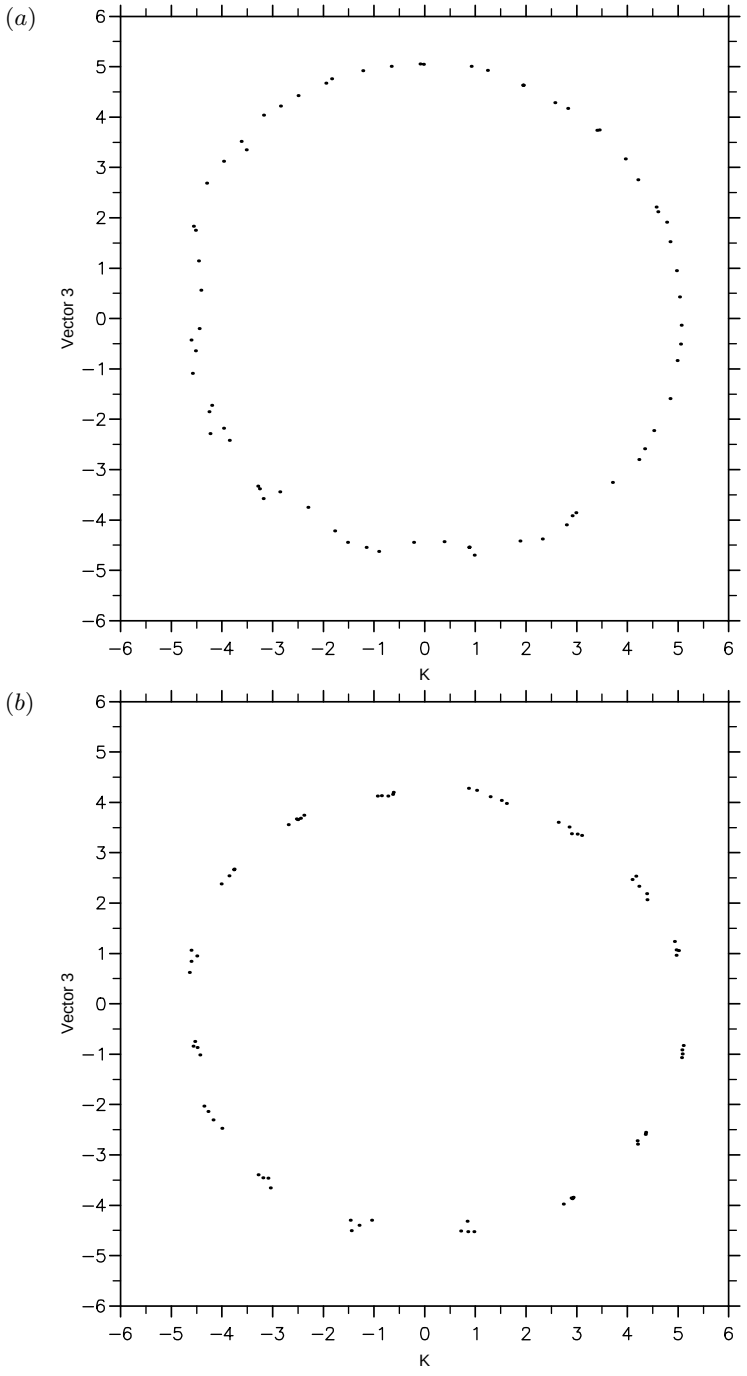

Figure 11. 3MAV-r regime, case (h): Poincaré sections at vector 1 = 0 from phase space reconstruction, (*a*) first half, (*b*) second half of experiment.

$(m|m{+}1|1)$, while the harmonic mechanism relies on the triad $(2m|m{-}1|m{+}1)$. In the present case of a dominant zonal mode $m = 3$, analysing the phase coherence of the

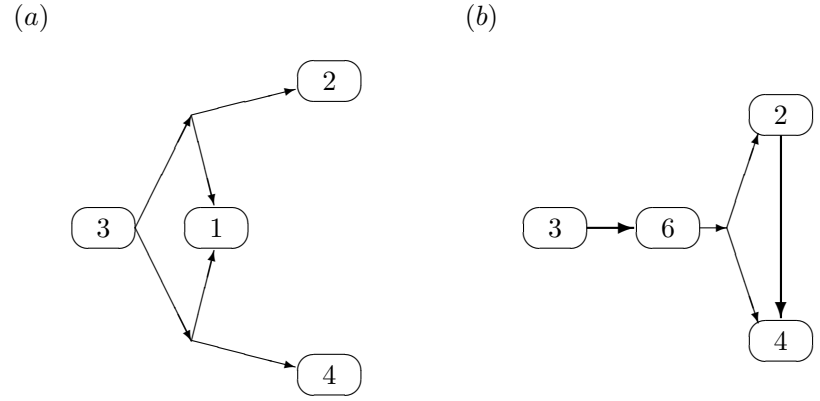

Figure 12. Wave interaction mechanisms for the sideband coupling, (*a*) via the long wave, and (*b*) via the harmonic mode.

triads (3|2|1), (4|3|1), and (6|4|2) will give indications about the relative importance of the respective mechanisms.

Investigating the phase coherence of the steady wave $m = 3$ with other zonal modes confirmed the findings by James *et al.* (1981). Even though the amplitude of the sidebands was typically less than 10% of the dominant mode, a strong sideband phase locking with $\Phi_3 \approx 3\pi/4$ was observed. The triad locking probability density function showed that the sideband coupling was consistently associated with triad phase locking of the harmonic triad with $\varphi_{6-4-2} \approx 3\pi/2$. Together with the observed phase coupling of the first harmonic to the dominant wave number through self-interaction with $\varphi_{6-3-3} \approx 3\pi/4$, one obtains $\Phi_3 = \varphi_{6-4-2} - \varphi_{6-3-3} \approx 3\pi/4$.

The most effective phase coupling in the 3AV and 3MAV flows was generally achieved by the lower sideband/long-wave triad, (3|2|1), while the upper sideband/long-wave triad, (4|3|1), and the harmonic triad, (6|4|2) typically showed much less pronounced phase locking. This would suggest that in these vacillating flows the harmonic triad proposed by James *et al.* (1981) is less important than the long wave. Possibly the single triad (3|2|1) or the sideband instability suggested by Hide *et al.* (1977) is a significant nonlinear wave interaction in the observed amplitude vacillation.

A reversed scenario, however, is suggested for the isolated 3AV regime for very large Θ, above the IV regime. Only the harmonic triad revealed any noticeable triad phase locking, supporting—as for steady waves—the interaction mechanism after James *et al.* (1981). The long wave triads, otherwise preferred by vacillating waves, showed no evidence for coherent wave coupling.

Since the resonance condition for wave triads, equation (2.2), depends on the amplitude of the interacting modes, it can be expected that the strength of phase coupling varies over time in time-dependent flows. RBJS noted the necessity for an amplitude threshold to observe significant phase locking. They attributed this to the fact that noise made the reliable determination of wave phases impossible for small amplitudes. In the present study the effective noise threshold was about 0.01 K, below which no meaningful phase could be computed. Above this noise threshold, however, the phase locking functions showed phase coherence only over part of a vacillation cycle. Usually the phase locking was strongest when the secondary modes

were relatively strong. Using a higher, dynamical, threshold for the evaluation of the phase locking density showed much increased phase coherence. The value of the dynamical threshold depended on the wave number of each component and the particular flow examined, but was almost always well above the noise level with values of the minimum locking amplitude up to $A_i^c \approx 0.2\,\mathrm{K}$ for the secondary modes with wave number i, compared to a total amplitude range of $0.03 < A_i < 0.4\,\mathrm{K}$ in the particular example in figure 9*b*. The dominant mode, $m = 3$, was always above any threshold for moderately vacillating flows. Only in the 3MAV-r regime did the amplitude of $m = 3$ drop below its dynamic threshold of $A_3^c \approx 0.3\,\mathrm{K}$ for parts of the vacillation cycle.

Occasionally the dynamical threshold for locking in the strongest triad was of the order of, or less than, the noise level. One of such cases was the ultra-low frequency modulation in case (e), which altogether showed much stronger phase coupling compared to the other more typical 3MAV flows; all triads showed strong phase coherence, and the lower sideband-long wave triad was phase-locked for the entire dynamic range of the modes $m = 1, 2$, and 3 above the noise level. In the 3MAV-r regime, some flows were observed where the triad (3|2|1) would be active for all amplitude ranges of the waves, though the value of φ_{3-2-1} would change with the amplitude of $m = 3$. In this case the locking density would peak at values from $\varphi_{3-2-1} \approx 3\pi/8$ to $\varphi_{3-2-1} \approx 5\pi/8$ during phases of a strong mode 3, but when $m = 3$ was weak it would peak at $\varphi_{3-2-1} \approx \pi$.

When frequency locking was observed between the wave drift of the dominant mode and its vacillation in any of the 3AV and 3MAV regimes, enhanced phase locking between sidebands and other waves was observed, especially for the harmonic triad. The value of Φ_3 and φ_{6-4-2}, however, varied for different amplitude ranges. For strong sidebands $\Phi_3 \approx 7\pi/4$ and $\varphi_{6-4-2} \approx \pi$, but with weak sidebands, the phase relation changed to $\Phi_3 \approx 3\pi/4$ and $\varphi_{6-4-2} \approx 7\pi/4$.

(*d*) *Intermittent bursting*

Upon increasing Θ (or $\mathcal{T}$) from the 3MAV regime, the modulation of wave 3 became more pronounced and less regular, and the weaker modes became stronger. In particular mode $m = 2$ showed intermittent large-amplitude bursts, which coincided with the collapse of the vacillation of $m = 3$, followed by an approximately exponential recovery of the vacillation. This behaviour, and the bursting of $m = 2$, can be seen in the time series of the amplitude of modes $m = 2$ and 3 in this regime in figure 13*a* (case i).

As one moves further into the region of parameter space labelled 3/2I in the regime diagram in figure 2, these bursts become more frequent and stronger. The average frequency of the bursts, ω_i, was observed to be—like ω_d—primarily a function of the Grashof number. The best regression was obtained for a power law increase of ω_i with Gr above a critical value Gr_c (see figure 13*b*), of the form

$$\omega_i \propto \gamma^{0.7\pm0.1} \tag{6.2}$$

with $\gamma = Gr - Gr_c$. On the basis of these data, the critical value Gr_c was bounded by $1.6 \times 10^6 \leqslant Gr_c \leqslant 1.7 \times 10^6$. A value of $Gr_c = 1.66 \times 10^6$ was chosen for the scaling, resulting in a correlation coefficient of 0.968, and a formal error for the exponent of ± 0.04. Including the uncertainty in Gr_c results in the quoted uncertainty of ± 0.1.

The phase locking appeared to divide the regime into two parts, the regular subregime at smaller Θ and larger $\mathcal{T}$, which had regular bursts at relatively high burst

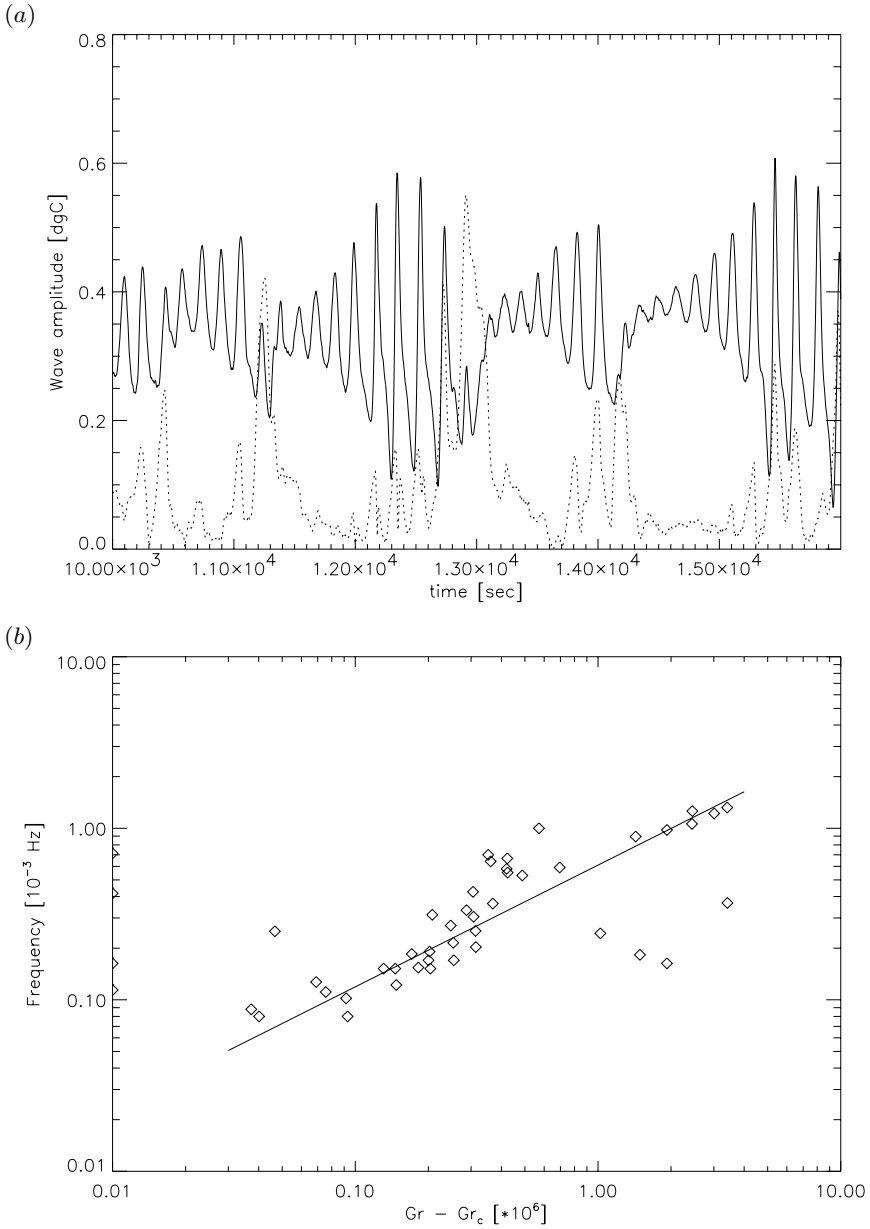

Figure 13. 3/2I regime, case (i): (*a*) time series of wave amplitudes of modes $m = 3$ (solid line) and $m = 2$ (dashed line), (*b*) scaling of the burst frequency with Gr. The regression curve has a slope of 0.71.

frequencies, and the more irregular 3/2I at larger Θ and smaller $\mathcal{T}$. The regular subregime showed essentially the same phase locking as the 3MAV flows with strongest coupling in the lower sideband/long wave triad (3|2|1), but in the less regular 3/2I both the sideband locking and the phase locking were much reduced.

Phase space reconstruction using multi-variate SSA reveals a trajectory with a roughly toroidal structure (figure 14*a*) for the 3MAV regime. The 'wall' of the torus,

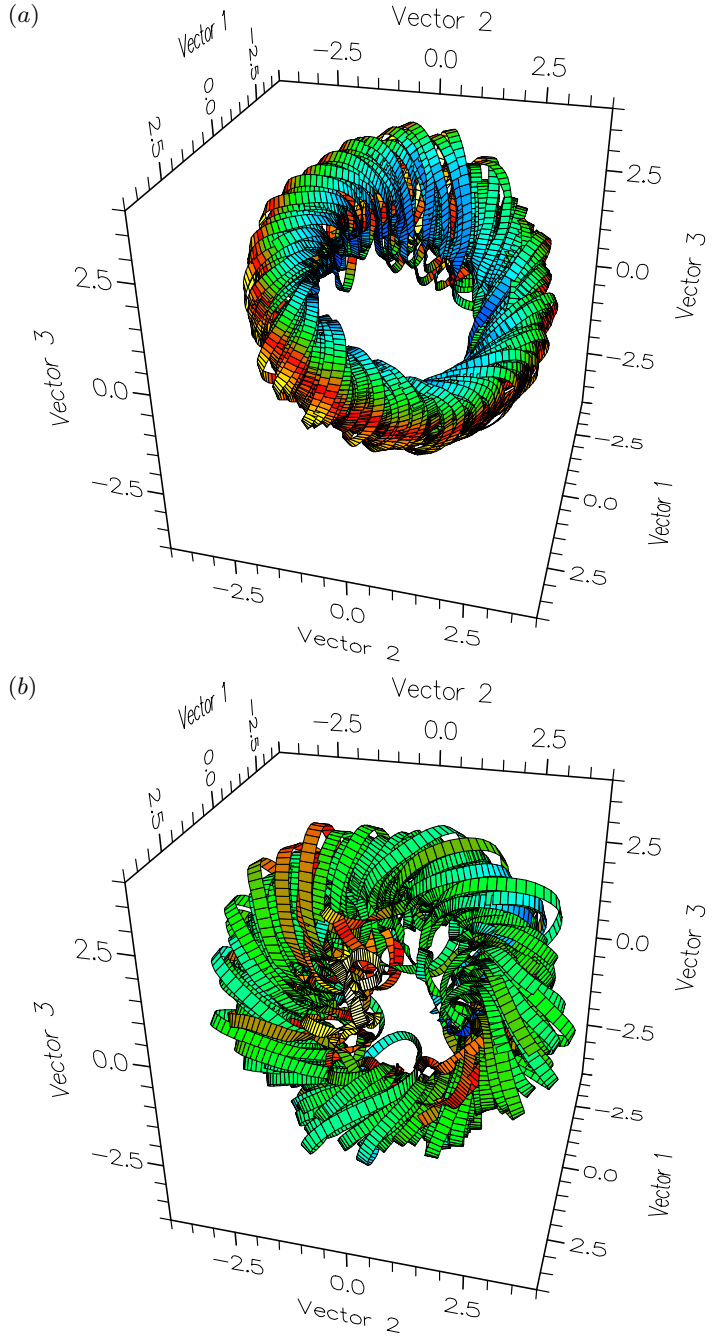

Figure 14. 3MAV (case d) and 3/2I regimes (case i): phase portraits of (*a*) a 3MAV flow and (*b*) a 3/2I flow.

however, is thicker than can be accounted for by experimental noise. Besides the 'fuzzy' torus, the return map of successive values of eigenvector 2, shown in figure 14*c*, has two clusters of points which indicate that the progression around the torus is interrupted at certain phases of the pair of eigenvectors 1 and 2. The thickening

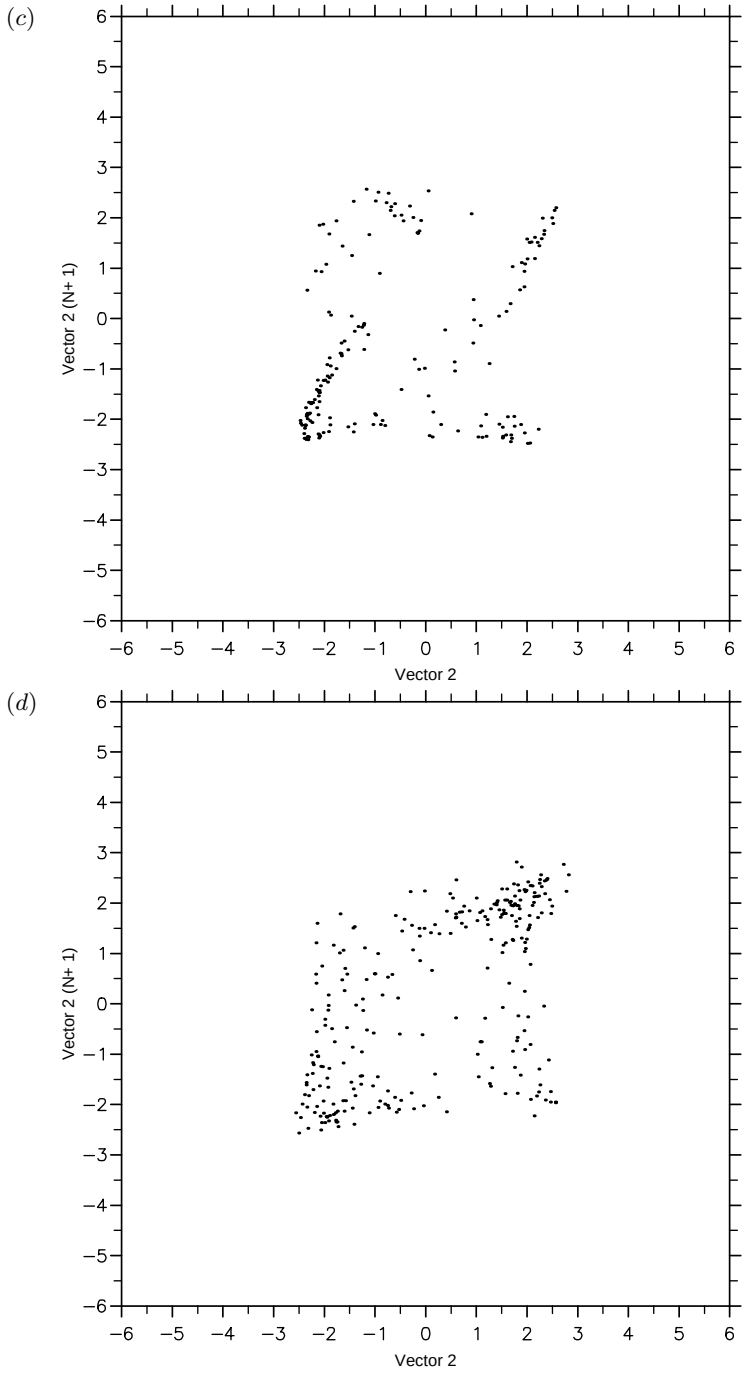

Figure 14. *Cont.* (*c*) and (*d*) their respective return maps of Poincaré sections at vector 1 = 0.

of the torus wall becomes more pronounced as one moves into the 3/2I regime, both in the phase portrait in figure 14*b* and in the return map of the Poincaré section in figure 14*d*. An estimation of the Correlation dimension using the Grassberger–Procaccia algorithm showed for all experiments in these two regimes a convergence

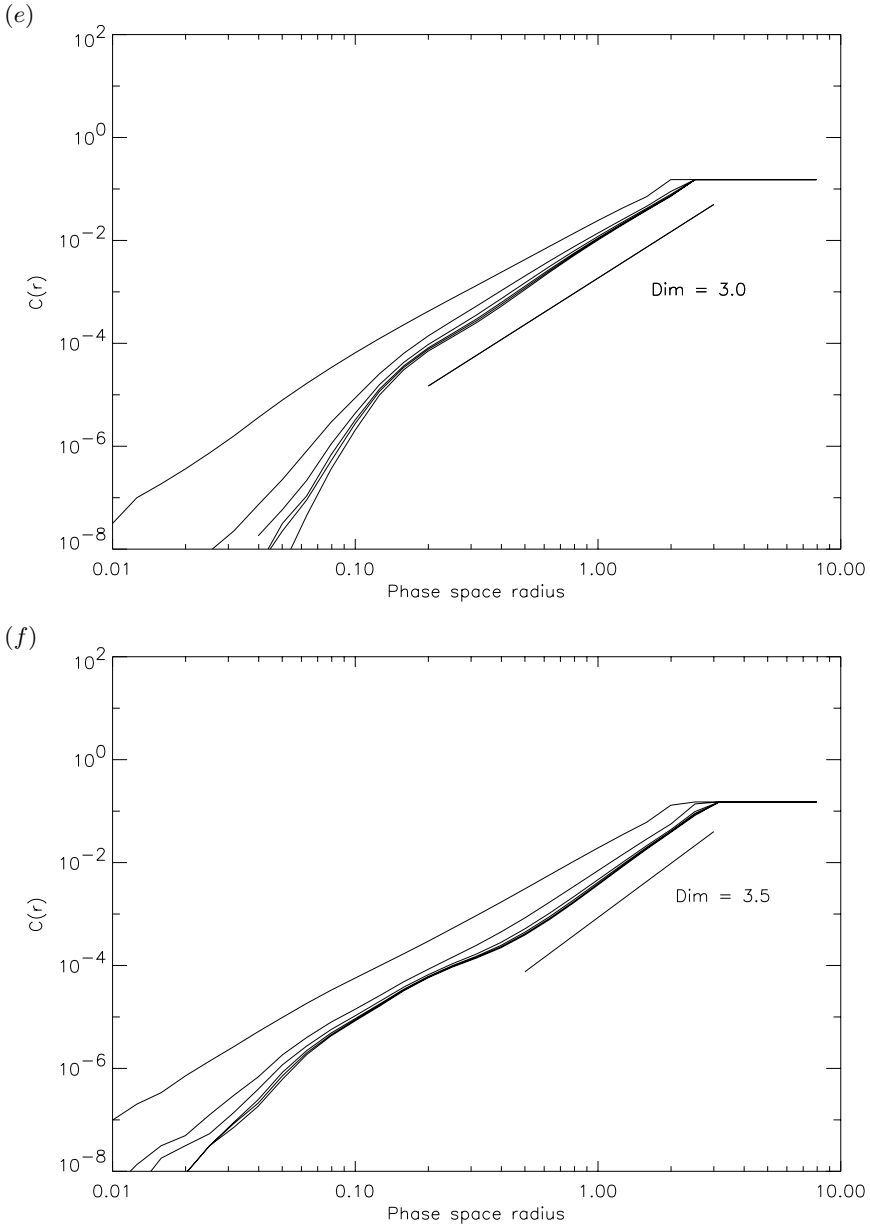

Figure 14. *Cont.* (*e*) and (*f*) their respective correlation integrals.

of the correlation integral with increasing embedding dimension, but while the 3MAV showed a large scaling region with $d_c \approx 3$ (figure 14*e*), the 3/2I regime showed a non-integer slope between $d_c = 3.1$ and $d_c = 3.5$ (e.g. figure 14*f*). The largest Lyapunov exponents were estimated following Wolf *et al.* (1985) and found to be significantly positive for flows in the irregular 3/2I regime with $\lambda_1 = 6 \ldots 8 \times 10^{-4}$ bits s^{-1}. The MAV flows discussed above seemed to be quasi-periodic or only weakly chaotic, with λ_1 either within the error level or $\lambda_1 \lesssim 4 \times 10^{-4}$ bits s^{-1} respectively.

Frequency locking was very rare in the 3/2I regime. Only one instance (case j) of

complete frequency locking was found in the present series of experiments. In this case, ω_i, ω_d, and ω_v, were locked in a ratio $1:1:4$. In addition to peaks at $\omega_{\mathrm{d},i}$, ω_v, and their sums and differences, the power spectrum also showed a distinct peak at $\omega_i/2$ indicating that the bursts were period-doubled. The difference in amplitude between successive bursts, however, did not remain constant, but was modulated over time. As can be seen in the time series of mode $m = 2$ in figure 15*a*, the difference between successive bursts grows gradually over time until, suddenly, successive bursts become equal, after which the difference starts to grow again. The phase portrait and its Poincaré section (figures 15*b*, *c*) show a limit cycle which is stretched into a flat ribbon. The second return map in figure 15*d* of the Poincaré section shows an increasing branch which corresponds to the gradual growth of the subharmonic, and a few points corresponding to the collapse of the subharmonic to equal bursts. The increasing branch forms a quadratic channel with the diagonal which is characteristic of intermittency type III (Bergé *et al.* 1984) but, since no more frequency-locked 3/2I flows were observed, it was impossible to prove that this is indeed a case of type-III intermittency.

(*e*) *Attractor switching*

In a range of parameters intermediate between the 3/2I, the 3MAV-r and the 2SV regimes, a flow type was observed which was characterized by a change of the dominant wave number at irregular intervals. This flow regime, in which the dominant wave number switched back and forth between $m = 2$ and $m = 3$, is denoted here as '$m = 2 - 3$ Alternating' (2-3A) in the regime diagram in figure 2. The $m = 2$ part of the flow was always similar to the 2SV flow described above in § 5, while the $m = 3$ part was similar either to the 3/2I flow described in § 6 *d* or, for large Θ, to the 3MAV-r flow described in § 6 *a*. The time series of wave amplitudes for $m = 2$ and $m = 3$ in figure 16*a* (case k) shows one switching event from $m = 3$ to $m = 2$, and a change back to $m = 3$ *ca.* $1000\tau_0$ later. The interval between two wave number changes ranged from several minutes to about 10 h.

The typical time interval between wave number changes was longer at parameter values closer to the adjacent flow regimes. The closer the parameters were to the 2SV regime, the more time the flow spent in the $m = 2$ state, and vice versa. This is illustrated in figure 16*b* which shows the relative residence time in $m = 3$, T_3^r, over a range of Gr. T_3^r is the fraction of the experiment during which the dominant wave number was $m = 3$. Though the scatter on the graph in figure 16*b* is considerable, using Gr, rather than any other function of $\mathcal{T}$ and Θ, nevertheless seemed to give the best representation of the data.

While the transitions between the 2-3A and 3MAV-r regimes and between the 2-3A and the 2SV regimes were very abrupt, the transition between the 2-3A and 3/2I regimes was much less distinct, being associated with a gradual increase in the amplitude of the $m = 2$ bursts as $\mathcal{T}$ or Θ increased, until occasionally $m = 2$ became strong enough to dominate the flow for a significant time.

Phase space reconstructions of the 2-3A flow show two distinct and mutually orthogonal oscillation patterns, associated with the $m = 2$ and the $m = 3$ flow types respectively (see figure 17*a*). Using multi-channel phase space reconstruction the eigenvectors not only show the principal oscillations of the flow but also the spatial structure of these oscillations. Eigenvectors 1 and 2 (see figure 17*c*), for example, have the spatio-temporal structure of a travelling wave $m = 2$, while eigenvectors 3 to 6 (e.g. figure 17*d*) have the structure of a travelling, vacillating $m = 3$ wave. The

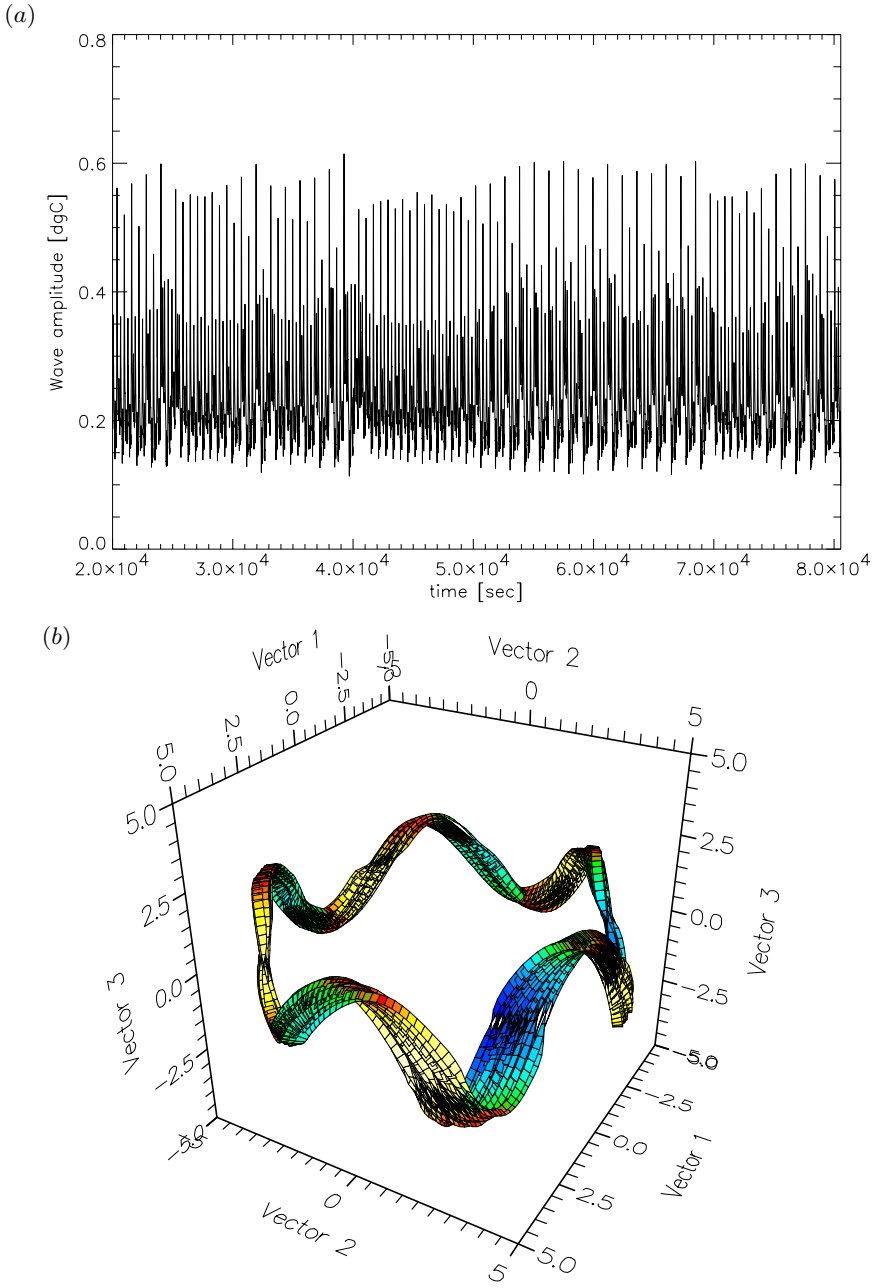

Figure 15. 3/2I regime, case (j): (*a*) time series of wave amplitude of mode $m = 2$, (*b*) phase portrait.

trajectory can be seen in figure 17*a* to orbit for part of the flow in the space spanned by eigenvectors 1 and 2 with only small amplitude in the other eigenvectors, and for the other part in the space spanned mainly by eigenvectors 3 to 6, with very small amplitude in eigenvectors 1 and 2. These two separate regions in phase space are joined by very rapid transitions between them.

As an alternative way of visualizing the transition between the distinct wave states,

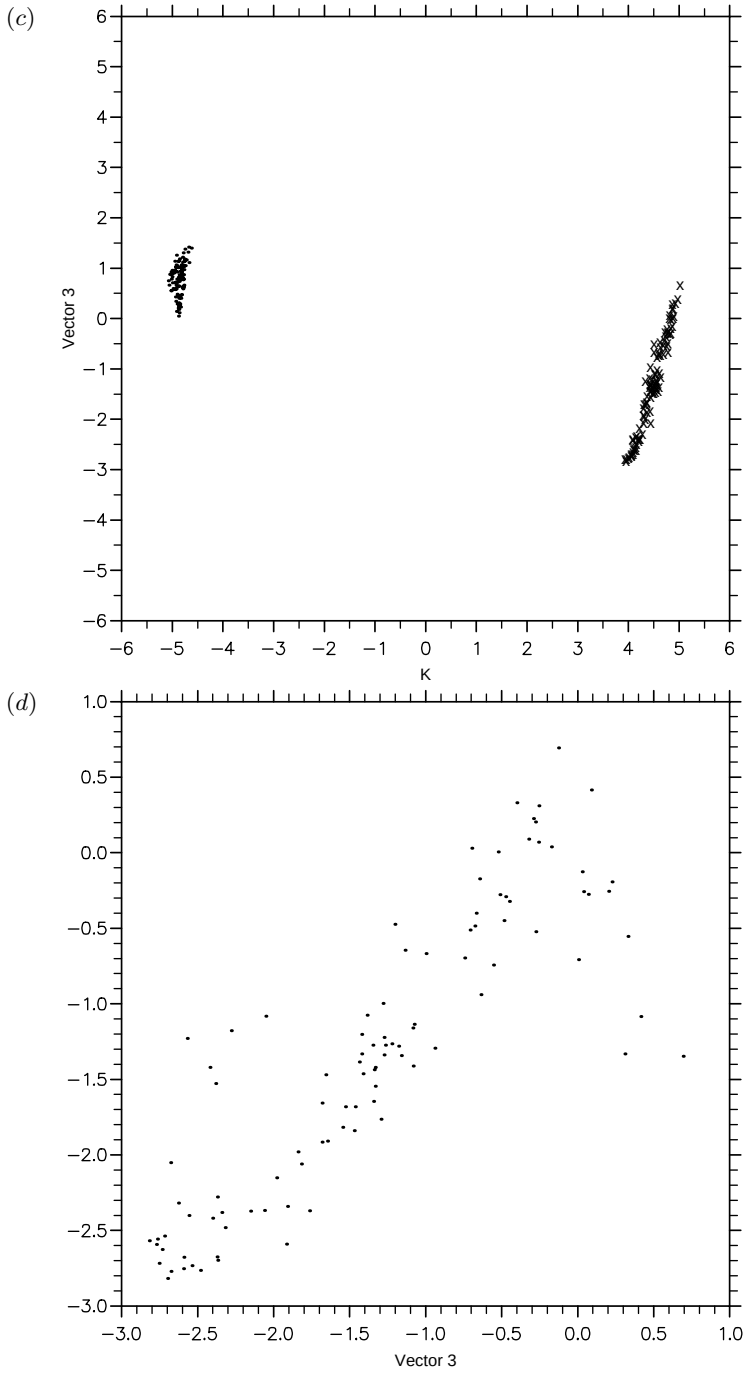

Figure 15. *Cont.* (*c*) Poincaré section at vector 2 = 1.0, and (*d*) its *second* return map.

figure 17*b* shows a phase portrait in a space defined by the total amplitude of each spatial pattern, for which pairs of eigenvectors represent components of a single complex pair. Based on the correspondence of the nonlinear principal components to linear Fourier waves, the sum of the squares of a pair of principal components corresponds

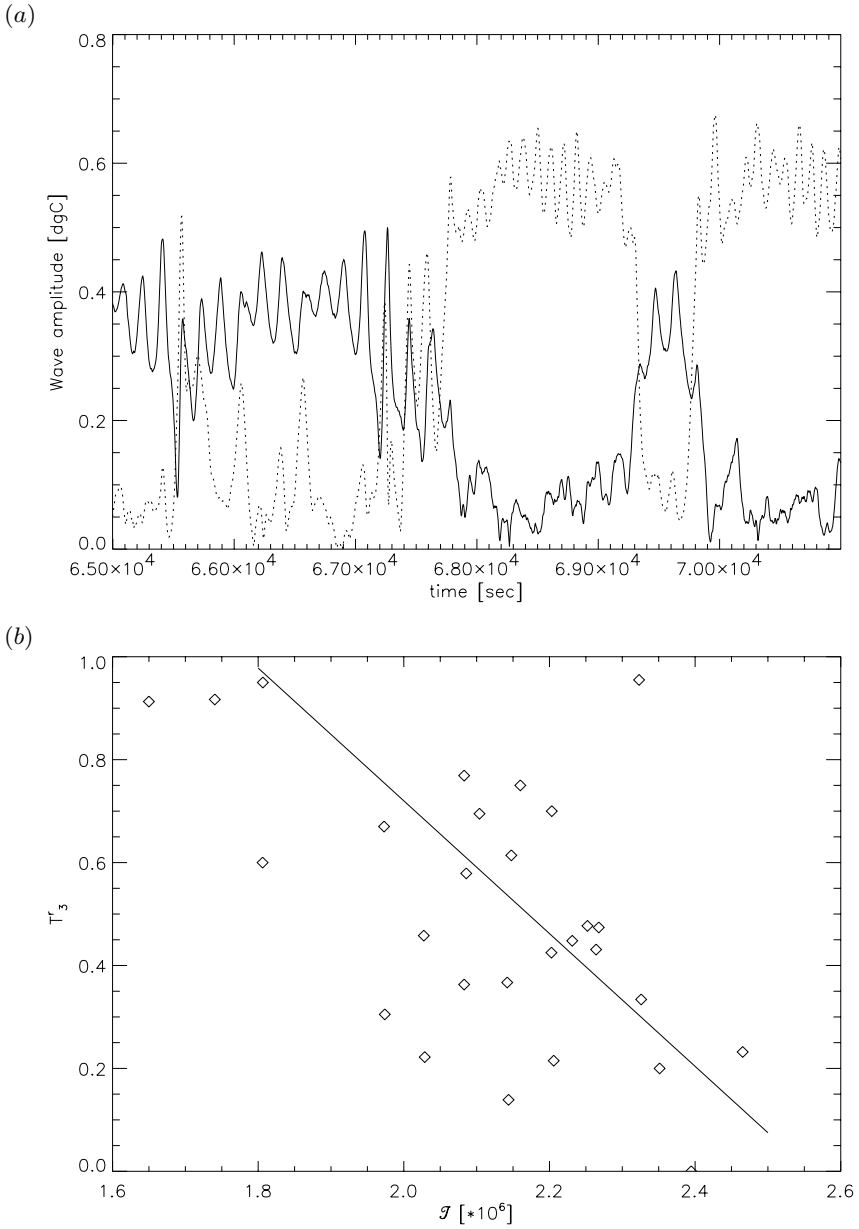

Figure 16. 2-3A regime, case (k): (*a*) time series of wave amplitudes of modes $m = 3$ (solid line) and $m = 2$ (broken line), and (*b*) relative $m = 3$ residence time, T_3^r *vs* Gr. The regression line has a slope of -1.29.

to the amplitude of each wave-like oscillation. The irregularly vacillating 2SV part of the flow thus collapses onto the cluster on the top, and the stronger vacillation of the 3MAV part is represented by the noisy cycle on the bottom. This picture suggests the existence of two separate states joined either by a heteroclinic cycle or by the mutual erosion of their respective basins of attractions through an attractor-merging bifurcation; two possible mechanisms which will be further discussed in § 8 *c*.

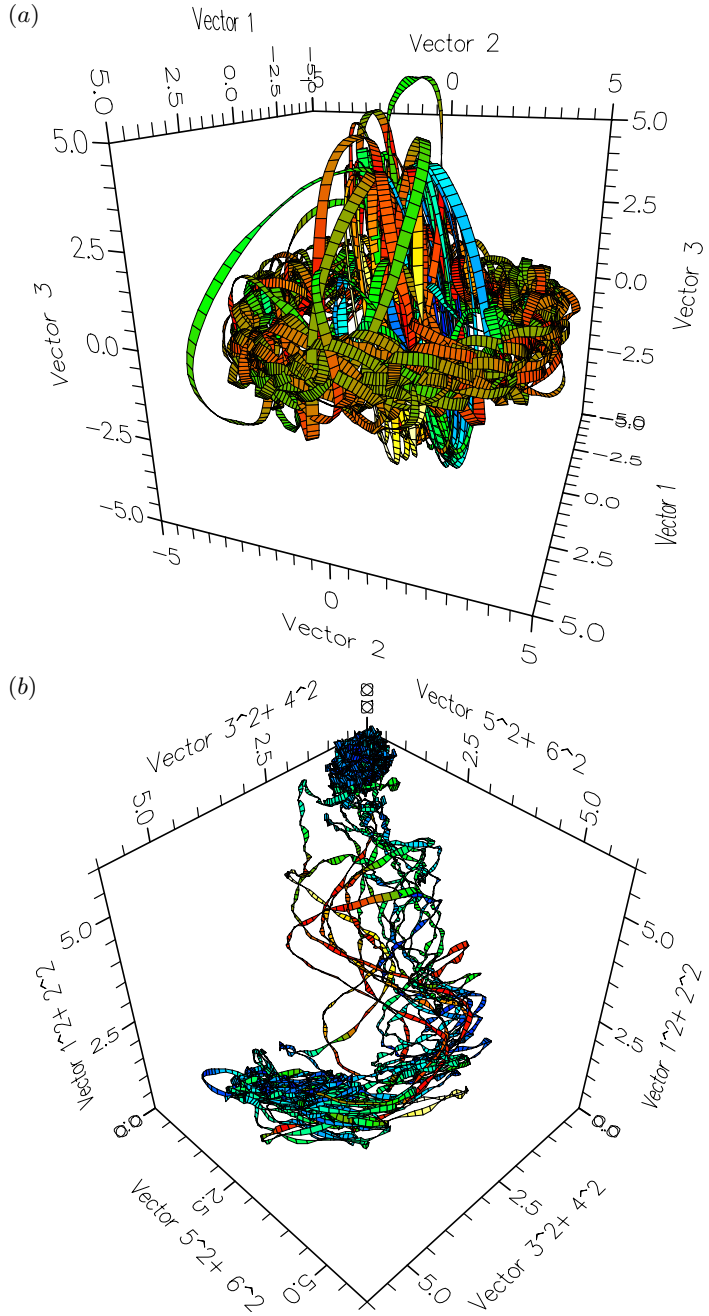

Figure 17. 2-3A regime, case (k): (*a*) phase portrait of thermocouple data, (*b*).

The Grassberger–Procaccia algorithm applied to the temperature data resulted in several small scaling regions with scaling exponents of $d_c \approx 2.3$, 4.5, and 1.5, as given in figure 17*e*. From well behaved low-dimensional dynamics one would expect the dimension of the heat flux attractor to be one less than the attractor from temperature data if the phase of the wave were unimportant (the heat flux is an azimuthally integrated quantity) or an identical attractor dimension, if the modu-

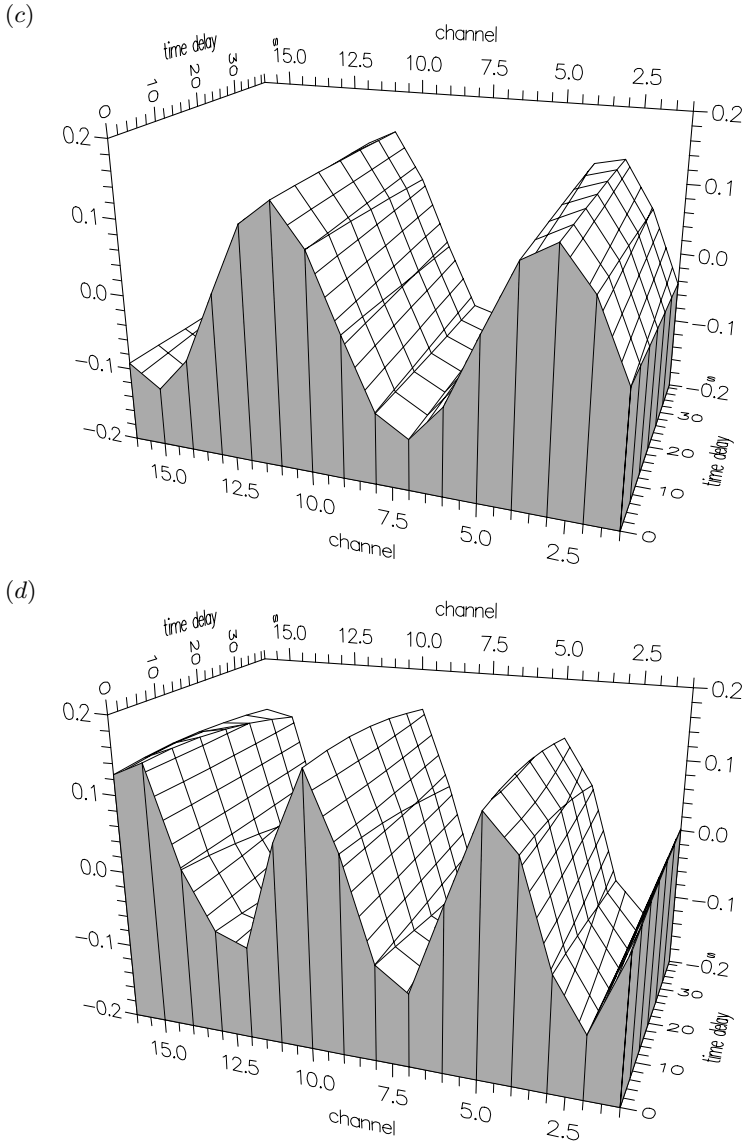

Figure 17. *Cont.* (*c*) First and (*d*) fourth eigenvector of (*a*).

lation of the amplitudes were caused through phase locking. Although converging, the correlation integral from the heat flux data in the 2-3A regime had only two scaling regions, as shown in figure 17*f*; one with a much higher scaling exponent of $d_c \approx 5.7$ which is similar to the scaling of the correlation integral for the heat flux in the 2SV regime (cf. figure 8*d*), and another scaling region at small phase space radii with the same scaling as the thermocouple data of $d_c \approx 1.5$. This suggests that, if any, only the smallest region shows any reliable dimension estimate, while the others scaling regions are caused by the strong inhomogeneity of the attractor in the phase space. The heat flux shows only one additional scaling region because the two oscillations corresponding to the two different wave states are in the same plane of the phase space, whereas the temperature data of the two states span orthogonal

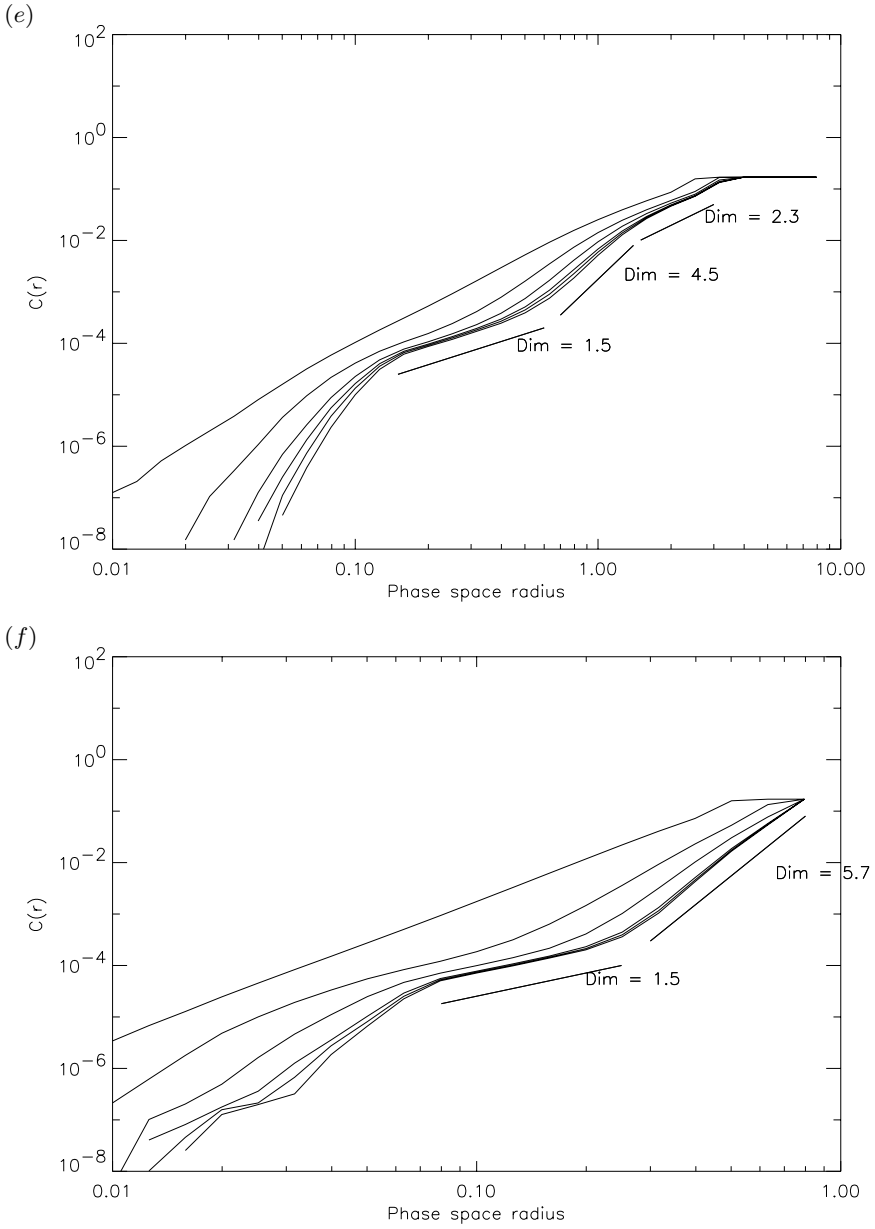

Figure 17. *Cont.* (*e*) Correlation integral for the thermocouple data, and (*f*) correlation integral for the heat flux.

subspaces. If the dimension of $d_c \approx 1.5$ were true then this would imply that there is sufficient coupling of the drifting waves to the convection chamber, such that information of the phase drift is transferred to the total heat flux. In the phases of the Fourier components, however, no clear phase could be associated with the wave number transitions, which indicates that the essentially stochastic fluctuations of the 2SV state (cf. § 5) might play an important role in this flow regime.

7. Stationary waves

An accidental occurrence of an air bubble in the convection chamber produced a topographic perturbation which resulted in the freely drifting waves becoming stationary in the reference frame of the apparatus. When the bubble was small no change in the flow was detected, but above a critical size the waves stopped drifting along the channel. Neither the dominant wave number nor the vacillation of its amplitude were significantly affected by this perturbation. This forced removal of a free frequency, however, altered the subsequent bifurcation sequence drastically. The initial flow, case (l), was on a noisy limit cycle (figure 18*a*) which, under increasing $\mathcal{T}$, bifurcated to a noisy period-doubled limit cycle in case (m) (figure 18*b*). The spread of the trajectory in the plane of the limit cycle is much greater than any instrumental noise and must arise from transient or spatially localized fluctuations. A period-4 cycle was also observed on further increase of $\mathcal{T}$, but neither a period-8 flow nor any other transitions were found in the range of parameters studied. Although there was evidence for intermittency of type III in the 3/2I regime and for torus-doubling in the 2+3IV regime, the stationary waves were the only flows which showed a clear sequence of two period-doubling bifurcations. Similar to the 2SV flow (cf. § 5), the noisy limit cycle is reflected in only very small scaling regions of the correlation integral, with $d_c \approx 1.5$ in the period-1 flow and $d_c \approx 2.4$ in the period-2 flow. The rather large value in the period-2 flow suggests that the dimension calculations are unreliable in these cases, especially since the Lyapunov exponents for both cases are much smaller than their uncertainty.

8. Discussion

We have presented a series of experiments with the thermally driven rotating annulus with a flat rigid upper lid and base. The experiments were primarily aimed at exploring multi-mode flows in the regular wave regimes with moderate dominant wave numbers. The previous study by RBJS had shown the existence of low-dimensional chaos in the guise of a modulated amplitude vacillation with significant power in the azimuthal side bands and consistent phase locking of these sidebands to the dominant mode. The present study has essentially confirmed the findings of RBJS, but has also revealed a range of new complex flow types close to wave number transitions.

An overall feature of the waves was their dependence on three main interdependent non-dimensional numbers, the Taylor number $\mathcal{T}$, the stratification parameter Θ, and the Grashof number $Gr \equiv \mathcal{T}\Theta$. While the relevance of $\mathcal{T}$ and Θ has long been known, the observed functional dependence on Gr of some free frequencies has not been reported previously. In particular the drift of the wave patterns through the annular chamber appeared to be a function of Gr only. In addition, the bursting frequency in the 3/2I regime also seemed to scale with Gr. In agreement with previous studies, the vacillation frequency in AV and MAV flows, but not in SV, was found to scale with $\mathcal{T}$. Many of the regime boundaries appeared to align approximately with lines of either constant Θ or constant Gr. With the thermal wind relation, Θ is a measure of the Rossby number, where the advection by the shear flow associated with the temperature gradient is compared with the Coriolis term. The Grashof number measures the buoyancy force with respect to viscous dissipation, the main forces in free (buoyancy-driven) convection. If other forces are neglected, a small

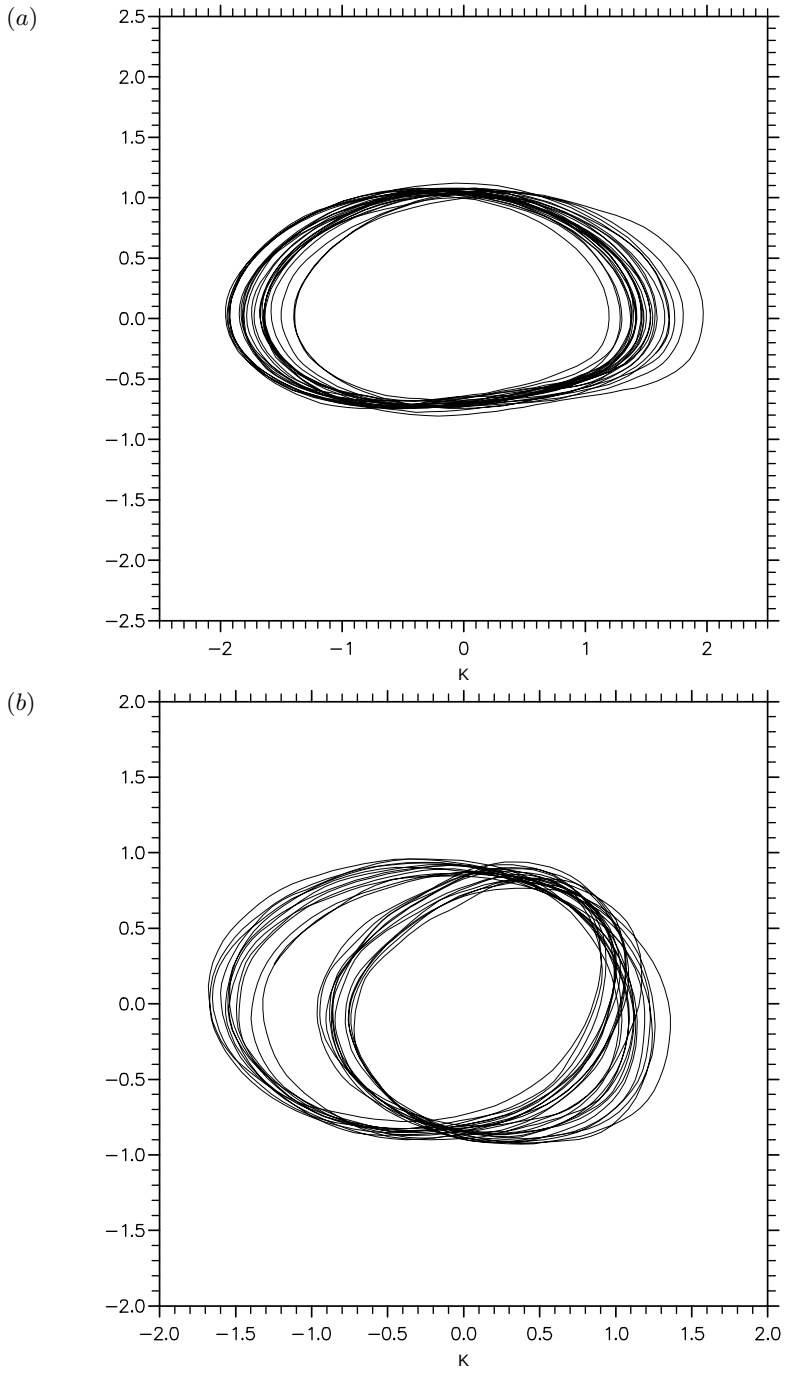

Figure 18. Stationary waves: phase portrait of (*a*) simply-periodic flow (case l), and (*b*) period-doubled vacillation (case m).

temperature contrast, and hence a small Gr, would result in weak convection. The heat transport by free convection in non-rotating fluids is primarily a function of Pr and Gr (Condon & Odishaw 1958). In the case of rotating convection in the annulus,

it seems that the strength of the thermal wind, measured by Θ, and the convection due to the balance of buoyancy and viscous dissipation, measured by Gr, have a strong influence on the dynamics. In contrast, the Ekman pumping, measured by $\mathcal{T}$, which is related to the Ekman number ($\mathcal{T} \sim E^{-2}$), appears to be less important in determining the timescales in the flow, except for the amplitude vacillation frequency.

One of the new features which we have observed was the transition from the lower symmetric regime at large Θ (i.e. close to the upper symmetric regime) to the dispersive regime D. For smaller Θ the usual transition to steady waves was observed. The flows in the D regime showed irregular fluctuations of the amplitudes of the first four zonal modes drifting with relatively high phase speeds. A different regime of fast travelling irregular waves, called *weak waves*, has been known to occur at large $\mathcal{T}$ close to the transition from the upper symmetric regime to regular waves, above the theoretical marginal stability curve. In a numerical and experimental study by Jonas (1981) it was established that these waves lie beyond the classical Eady cut-off, and would grow from an instability due to the vertical variation of the symmetric flow. A stability analysis of a realistic flow profile near the D regime, taking into account both stratification and dissipation, might also show an instability not represented in the Eady model. For instance, effects from the side walls are usually ignored in theoretical models of baroclinic instability, assuming free-slip boundaries, but a recent stability analysis of a two-layer fluid by Mundt *et al.* (1995) included no-slip conditions at the side-walls. They found that, for a substantial range of parameters, a chaotic wave solution coexisted with the symmetric solution close to the linear stability boundary of the symmetric regime.

The improved control over the experimental conditions for very long durations in the present study has enabled us to investigate low-frequency mixed-wave states, which were observed within what was previously identified as the regular wave regime in regions between ranges of parameter space dominated by two different zonal modes. These multi-mode states arise from nonlinear wave interactions (e.g. 3/2I and 2+3IV) or from the merging of coexisting attractors due to the multiplicity of states in the baroclinic annulus. Our findings can be broadly classified into four main aspects: (*a*) frequency entrainment, (*b*) wave interactions, (*c*) chaos versus stochasticity and finally, arising from these, (*d*) multi-mode regimes with ultra-low frequency variability. These aspects will be discussed separately below in §§ 8 *a–d* respectively. The long duration of the experiments also revealed for the first time the existence of long-lived metastable transients, which could persist for much longer than typical experiments reported in the literature. In this light, some phenomena reported from previous studies might have to be interpreted with the possibility that they also were transients rather than the final equilibrated solution.

(*a*) *Frequency entrainment and stationary waves*

Generic MAV flows are weakly aperiodic, three-frequency flows with frequency components corresponding to the phase drift of the dominant wave pattern, the amplitude vacillation and a slow secondary modulation. By frequency locking, however, the number of independent free frequencies may be reduced to two, or even just one. Two types of frequency entrainment were observed, locking of ω_m to ω_d, and complete locking of all three frequencies, ω_m, ω_d, and ω_v. Previous studies have reported ambivalent evidence for the absence of frequency locking, lending support to the theoretical results of Rand (1982) from group-theoretical arguments which suggested a complete decoupling of amplitude and phase for wave-like disturbances in

axisymmetric containers. Already in 1969, Fowlis & Pfeffer (1969) observed a weak modulation of the amplitude vacillation when they used thermocouple probes, and they suggested that the modulation actually arose from interactions of the waves with the probes, which implies that phase and amplitude are not decoupled. Furthermore, Hide & Mason (1975) observed that in annulus flows with a free surface, where the wave pattern drifts at a timescale similar to the vacillation period, most flows showed locking of these two frequencies. Only in experiments with a rigid lid, in which the drift is an order of magnitude slower than the vacillation, is this frequency locking removed. In the present work both the occurrence of a modulation and the locking of the modulation and drift frequencies (which were of the same order) were very common, and it is suggested that small irregularities in the container and thermocouple ring perturbed the nominally circular SO(2) symmetry of the annular container, which are present in any physical system. It would furthermore be expected that the coupling of the waves to the container would show resonances when the symmetry group of the waves is a subgroup of the symmetry group of the container or vice versa. Since the thermocouple ring had D32 symmetry one might expect strongest coupling with flow whose symmetry formed a subgroup of D32, such as waves $m = 2$ or 4. The only modulated vacillation observed which satisfied this condition, was the 4MAV at very low Θ ($\Theta < 0.08$), and indeed, in all cases of that regime all three frequencies were observed to be locked to each other.

In general, however, nonlinear coupling of the vacillation and drift frequencies was much weaker than the coupling between the wave phase and the modulation. This is not surprising if the presence of probes enhances the occurrence of a modulation, as Fowlis & Pfeffer (1969) suggested. In a few cases, the vacillation frequency was also observed to assume an integer multiple of the drift frequency, and the flow became a limit cycle. In the main 3MAV regime, periodic, fully frequency-locked flows were interspersed among chaotic flows where at least the drift and primary vacillation frequencies were incommensurate. We suggest that in these cases we have observed parts of a 'devil's staircase', which was incomplete primarily because the mechanism of the coupling was very weak. We found evidence (case h) that the timescale of the onset of locking was of the order of, or longer than, the duration of the experiments. Also, locked and incommensurate states were sometimes found under identical conditions. If the experiment were left long enough at fixed parameters for locking to take place, together with minimum variations in Ω and ΔT to scan the parameter space, it might be possible to observe finite regions of locking in the form of Arnol'd tongues arranged in a devil's staircase as part of a generic transition to chaos involving frequency locking. Due to the timescales associated with the experiment, however, it was not feasible to test these ideas rigorously in the laboratory. Low-order numerical models, which in addition to the dynamics of baroclinic waves also include a weak coupling of the fluid with the container, might help to elucidate the problem of coupling caused by imperfections present in every practical system. An approach which is suggested here for further laboratory studies, is to reduce the timescale of drift-vacillation interactions by introducing controlled perturbations of the spatial symmetry with, for instance, false bases with topographic features consistent with specific symmetry groups (e.g. D4 or D3).

The resonance of the wave drift with the container is a possible reason, for example, that Ohlsen & Hart (1989*a*, *b*) observed locking and period-doubling in their experiments, yet found bifurcations through the quasi-periodic route in their numerical model. Their two-layer experiment had three probes aligned on one diameter, one

on the rotation axis and two at opposite sides three quarters out from the axis. This would cause a wave 2 perturbation, which could strongly interact with the $m = 1$ and $m = 2$ modes in their study.

In our cases of fully frequency-locked flow, which had essentially one free frequency left, period-doubling bifurcations were observed in a number of regimes (3MAV, 3/2I, stationary waves), whereas a doubled torus in two-frequency flow was very rare, being observed only in the small IV regime.

(*b*) *Wave interactions*

It was observed in almost all experiments that the phases of the dominant zonal mode m and its sidebands $m \pm 1$ were locked, or at least partially locked, such that the waves drifted with the same angular frequency rather than with the same phase speed, as one would expect of decoupled waves. In our experiments, the time-averaged strength of this locking was measured by the sideband locking probability density function ρ_m. This, and the triad locking probability density function $\rho_{m-m'-m''}$, were found to be useful new tools in the analysis of different proposed wave interaction mechanisms.

Two distinct wave interaction scenarios have been proposed in the past for the coupling of sidebands, one involving two *almost* resonant wave triads, the other combining the self-interaction of the dominant wave and one wave triad. In the present series of experiments, the results from the numerical simulations of a steady wave by James *et al.* (1981) were confirmed in certain cases, in that for *steady* waves, the harmonic triad (6|4|2) showed more persistent and pronounced phase locking than either of the long wave triads, (3|2|1) and (3|4|1). For *time-dependent* modes, however, the interaction scenario was more complex, partly due to the amplitude dependence of the resonance condition, with the result that the coupling strength varied constantly in the different triads. The flow could in this case show a complex alternation of phase locking scenarios as the wave amplitudes of the modes progressed through their vacillation cycles.

The region of time-dependent $m = 3$ waves appeared to be divided into two parts, one at large Θ ($\Theta \gtrsim 0.9$) and one at smaller Θ ($0.2 \lesssim \Theta \lesssim 0.8$), separated by a tongue of D_2 flow and the interference vacillation. At smaller Θ the long wave triads, especially (3|2|1), showed the strongest coupling, but at large Θ the 2+3IV and 3AV regimes showed strong phase coherence in the harmonic triad. The transition from the IV regime to the D_2 regime occurred through a torus-doubling and the subsequent break-up of the T^2-torus of the IV flow. At this transition the phase locking changed abruptly from $\varphi_{6-4-2} \approx \pi/2$ to $\varphi_{6-4-2} \approx 5\pi/4$, which suggests that the harmonic triad is an essential feature in stabilizing the 2+3IV and 3AV regimes.

For the more irregular 3/2I sub-regime the phase coherence was generally very weak, and it seemed that in this regime wave-wave interactions are less important than wave-zonal flow interactions. These findings are supported in numerical simulations using a two-level quasi-geostrophic model by Früh (1996).

Frequency entrainment of the drift frequency to an integer fraction of the vacillation frequency also modified the mutual phase locking of the triad components. In the one directly observed case of onset of frequency entrainment it was the drift frequency rather than the vacillation frequency which became entrained, and such a forced change of the drift frequency would be expected to affect significantly the resonance conditions. The result of frequency entrainment was always a marked enhancement in the phase locking, especially of the harmonic triad.

(*c*) *Chaos versus stochasticity*

Previous studies by Guckenheimer & Buzyna (1983) and RBJS have shown, by calculating attractor dimensions and Lyapunov exponents, that amplitude vacillations and (in the case of RBJS) modulated amplitude vacillations follow low-dimensional dynamics, where the AV flows are quasi-periodic and the MAV flows usually chaotic. The low-dimensional character of these flows was subsequently confirmed when Smith (1992) successfully constructed a nonlinear radial basis function predictive model of one of the chaotic MAV flows observed by RBJS, assuming a finite embedding dimension. In the present study, not only the MAV but also the 3/2I regime, which appeared to develop from the MAV flow, possibly through a homoclinic bifurcation, were consistent with low-dimensional dynamics. Correlation integral calculations showed scaling with small non-integer values of $d_c = 3$ to 3.5, together with positive Lyapunov exponents for the aperiodic 3MAV and 3/2I flows.

RBJS have already shown, however, that structural vacillation flows behave quite differently. Independent dimension estimates, which were calculated from temperature and heat flow measurements, failed to give consistent answers. They argued that the SV arose not from a global, domain-filling instability, as for the AV, but from spatially localized instabilities. We have not only confirmed this result, but also found weaker but significant structural vacillation at much higher values of Θ, where RBJS, working with a different arrangement of thermocouple probes, had previously classified the flow as steady. The fluctuations of the wave amplitude, at around only 10% of the mean amplitude, were strong enough to destroy the scaling region in dimension calculations. This was reflected in the phase portrait which showed a limit cycle broadened by 'dynamical noise' which was much stronger than any measurement noise. The dynamics seemed to be divided into domain-filling and deterministic low-dimensional dynamics of the large scales on one hand, and fluctuations arising probably from localized transient instabilities on the other. It has been suggested that the observed oscillations are the manifestation of the wavering of the jet stream (Hide 1958; see also Hide & Mason 1975), which is detectable in thermal measurements but only barely perceptible in flow visualization data. While this is certainly possible, the amplitude of the oscillations seems too large to remain imperceptible in visual data. Also, steady waves were found for which the measured amplitude fluctuations were small enough to give satisfactory dimension estimates consistent with flow on a limit cycle. While the SV fluctuations destroy the scaling regions for dimension calculations, they still seem fairly regular with distinct peaks in the power spectrum, and the cause must be found in a dynamical instability rather than in purely random noise. If the growing disturbances are localized, they cannot be described by domain-filling 'normal modes' and therefore appear very high dimensional, or random at a practical level. These instabilities might have an atmospheric counterpart in the concept of 'optimal modes' (Farrell 1989), which are disturbances evolving locally at super-exponential rates while changing their shape. To investigate the precise structure of the SV flows one would need high-resolution spatial data, either from a dense thermocouple array, which would presumably affect the flow considerably, or from high-resolution flow visualization techniques.

The presence of high-dimensional transients may also have implications for the attractor switching 2-3A regime. If the attractor switching events were not due to stochastic perturbations, a heteroclinic cycle could be postulated. Though usually structurally unstable, a heteroclinic cycle can be stabilized by symmetries in the sys-

tem. Aubry *et al.* (1988), for instance, observed heteroclinic cycles in a turbulent wall layer. The presence of apparently irregular vacillation with an amplitude of about 10% of the mean amplitude makes it unlikely that a heteroclinic cycle could exist. Random perturbations, however, could cause transitions between disconnected stable solutions, as previously found, for instance between a limit cycle and a fixed point (e.g. Gaveau *et al.* 1992). A different possibility for attractor switching is a crisis, where two basins of attraction collide, described as attractor merging by Grebogi *et al.* (1987). The observations in the 3/2I regime would seem to support the mechanism of a classic attractor-merging crisis with the attractor of the 3/2I expanding, as shown by the increasingly stronger $m = 2$ bursts, until it hits its basin boundary and merges with the existing 2SV flow. One might speculate that the presence of the high-dimensional, essentially stochastic, fluctuations in the 2SV part of the 2-3A flow might induce the crisis before the actual attractor merging. We suggest therefore that the most likely scenario for the creation of the 2-3A regime seems analogous to a noise-induced crisis, such as that described by Sommerer *et al.* (1991), where stochastic perturbations would push the trajectory over the still existing, but only weakly repelling, basin boundary. The experimental evidence, however, is not conclusive for determining the exact mechanism, or even whether the apparently stochastic nature of the SV is essential.

A further investigation using simple idealized models of baroclinic waves, such as a low-order spectral model, might be able to investigate these hypotheses more rigorously. A purely deterministic model without any random forcing might be able to reproduce SV through the onset of vacillation of a second radial mode. Such a model, if found to reproduce a bifurcation sequency from flow similar to the 3/2I flow to an $m = 2$ structural vacillation via an intermediate regime of alternation between the 3/2I and 2SV caused by an attractor-merging crisis. On the other hand, a model without any higher radial modes cannot describe any structural vacillation. Such a numerical model, however, may show attractor switching when random forcing is added as a parametrization of the localized fluctuations in the $m = 2$ state. If an alternation between an $m = 3$ and $m = 2$ state were found in such a model, it would provide a possible mechanism for the 2-3A flow, either as a result of stochastically excited transition between two metastable states, or as a noise-induced crisis.

(*d*) *Multi-mode regimes and ultra-low frequency variability*

Ultra-low frequency variability in the atmosphere has been a focus of attention for some time. The timescales of interest are several months for weather prediction (Egger & Schilling 1983; James *et al.* 1994; Strong *et al.* 1995) and many years for climate studies (Rind & Overpeck 1993; Birchfield & Ghil 1993; Ghil 1994). While it is clear that some of the low-frequency motions in the atmosphere are driven by variations in the boundary conditions, such as sea-surface temperature patterns or solar radiation, there is also increasing evidence to suggest that internal dynamics of the extratropical atmosphere, without any external low-frequency forcing, can also generate variability on timescales much greater than the life cycles of individual synoptic and planetary waves. Our experiments have shown that a baroclinically unstable atmosphere may show variability on timescales from months to decades, which arises purely from the internal dynamics of multi-mode states. The multi-mode flows can be described as a competition between two or more domain-filling travelling wave modes, resulting in a low-frequency modulation of the wave amplitudes. This variability arises from nonlinear coupling of the waves through wave-wave or wave-

zonal flow interactions, or interactions of the fluid with the boundary conditions, sometimes leading to phase and frequency locking. These ingredients allow for a range of distinct behaviours, at least some of which are consistent with generic bifurcations of low-dimensional systems. The general structure of the regime diagram appears very complex, though we have suggested that widespread intermittent resonances and frequency locking between a limited range of spatial modes contribute to the apparently large variety of observed flow types.

For fairly small values of the Grashof number, Gr, a weak or moderate quasi-periodic or chaotic modulation (3MAV) could be observed with the slowest modulation towards small Gr. The transition from axisymmetric flow to *steady* waves at small Θ is consistent with a Hopf bifurcation, but all observations indicate that the transition from the lower symmetric regime to *vacillating* waves is far from the simple bifurcation sequence of a Hopf and a secondary Hopf bifurcation. It seems rather that the onset of the vacillation, which mostly depends on Θ, and the transition from axisymmetric flow to waves, which mainly depends on Gr, together give rise to a codimension 2 point with a homoclinic orbit indicated by the ultra-low frequency modulation.

Besides this ultra-low frequency 3MAV, two other regions of diverging timescales have been observed: the onset of the bursting of the 3/2I regime, and where the drift frequency of the 3MAV-r flows becomes very large, towards the transition to the 2SV and 2-3A regimes. The homoclinic behaviour associated with the bursting also persists when frequency-locking has occurred. Instead of a low bursting frequency we observed a low-frequency modulation of the bursting amplitude consistent with an intermittency bifurcation of type III. The bursting frequency in the generic 3/2I flows also was consistent with intermittency. Within the uncertainty of the exponent the estimated scaling of the burst frequency as $\omega_i \propto \gamma^{0.7}$ could be consistent with intermittency of either type-I ($\omega \propto \gamma^{0.5}$) or type-II ($\omega \propto \gamma$) (Schuster 1989). In a numerical study with a two-level model, Früh (1996) found solutions very similar to the 3/2I flows, in which the transition from single-wave solutions to multi-mode states was found to occur through intermittency.

While homoclinic bifurcations were the generally preferred bifurcations, other bifurcations occurred under much more specific conditions, with a striking absence of secondary Hopf bifurcations. The occurrence of perfectly regular T^2-tori was confined to large values of Θ, where the harmonic triad interaction seemed to be essential in establishing the regular 2+3IV and 3AV flows. This was also the region where a torus-doubling bifurcation was found. Otherwise, period-doubling bifurcations were restricted to flows with initial states which were one-frequency flows, either fully frequency-locked flows or stationary waves. The locking of ω_m to ω_d did not, however, result in quasi-periodic flow on a torus, nor did it seem to affect the bifurcations. The transition from the lower symmetric regime to steady waves along routes of constant Θ was consistent with a Hopf bifurcation, but the transition from steady to amplitude-vacillating waves was immediately to 3MAV rather than to 3AV flows—all observed 3AV flows for $\Theta < 0.8$ were in fact frequency-locked with $\omega_m = \omega_\mathrm{d}$ and $\omega_\mathrm{v} = n\omega_\mathrm{d}$ where n is an integer (typically between 3 and 6).

The last observed multi-mode regime with ultra-low frequency variability, the 2-3A regime, seemed to grow out of the 3/2I flow before the final transition to the $m = 2$ flow. At high values of Θ, the 2-3A regime was situated between the 3/2I and 2SV regimes, while at lower Θ the flow bifurcated directly from the 3/2I to the $m = 2$ regime and vice versa. The direct 3/2I↔2SV transition was hysteretic in

contrast to the 3/2I↔2–3A↔2SV transitions. Both transition scenarios involve two coexisting solutions, a 3/2I and a 2SV solution. The crucial difference seemed to lie in the stability of the $m = 2$ flow. For the hysteretic 3/2I↔2SV transition the $m = 2$ solution was stable, but in the 2-3A regime it acted like a saddle 'point'. It has been suggested above (§ 8 *c*) that the 2-3A regime is the result of a purely deterministic or a noise-induced attractor-merging crisis.

From analysis of observational data in the atmosphere (Plaut & Vautard 1994) it is widely accepted that variability on timescales less than a year, but longer than the intrinsic predictability of weather, is associated with switching between a small number of states or so-called 'weather regimes'. Plaut & Vautard (1994) found evidence that synoptic transients, such as baroclinic waves, may play a crucial role in the maintenance of this variability. Recent studies by Collins *et al.* (1995) of the general circulation of the Martian atmosphere found an irregular switching between two different wave states (similar to flow in the 2-3A regime but with zonal wave numbers $m = 1$ and 2) in the observed pressure time series from the Viking Landers, as well as in a general circulation model, though in these cases the dynamical annual and daily cycles of solar heating were significant.

Both low-dimensional deterministic dynamics as well as stochastic dynamics arising from localized instabilities were found to contribute to the complex flows observed in our laboratory experiments. These two mechanisms have also been used to explain the occurrence in climate models of long-term variability due to the internal dynamics. James & James (1989, 1992) used a simple atmospheric circulation model, with and without the annual cycle. Apart from a direct annual response in the presence of the seasonal cycle, the maximum variability occurred at periods of 10–40 years in either case, with and without the seasonal forcing. Pielke & Zeng (1994) observed significant variability on interdecadal timescales in a three-dimensional dynamical system derived by Lorenz (1990) as an example of a 'simplest possible general circulation model'. These deterministic models require the existence of a chaotic attractor, which would generate very long periods without the need for either long-period forcing or perturbations of solutions due to external noise. Different processes are invoked in stochastic models (Hasselmann 1976) where, in addition to the deterministic forcing terms, which represent climate dynamics on long timescales, random terms are also included to represent high-frequency components of the weather. The laboratory experiments described here, together with the numerical work proposed in § 8 *c*, could give some indication of the relative importance of low-dimensional chaotic dynamics and essentially stochastic localized perturbations on the large-scale flow of the middle latitude atmosphere.

9. Summary

The rotating annulus experiments presented here have shown a number of mixed-mode states, which exhibit a large variety of frequency and phase locking scenarios. We have defined a phase locking probability density function to analyse the strength of phase coupling of the phase locking of individual triads and the higher-order sideband coupling. Some regimes (3MAV and 2+3IV) showed clear indications that resonant triad interactions are important, while others (3/2I and 2-3A) seemed more to rely on the competition of two unstable modes through wave-zonal flow interactions. Two main triad interaction scenarios were observed, one involving the mutual harmonic mode of the two main modes, the other involving the long wave, $m = 1$. A

steady wave showed strongest coupling of its side bands through its first harmonic rather than via the long wave, but in vacillating flows the interactions were more complex. Due to the dependence of the coupling on the wave amplitudes, the wave interactions could lead to intermittent phase locking over only part of a vacillation cycle, or even to a complex competition between different triads. Generally, however, the regime diagram seemed to be divided into a larger region containing the 3MAV and 3MAV-r regimes, where the long wave triad (3|2|1) dominated, and a smaller region consisting of the interference vacillation (2+3IV) and a 3AV where their harmonics, (3|6) and (2|4|6), provided the coupling. These two regions were separated by the irregularly fluctuating dispersive wave regime D_2.

There was ample evidence for homoclinic bifurcations as an essential mechanism in organizing the regime diagram, with three critical points: (1) where the onset of vacillation and the transition from the symmetric regime to $m = 3$ flows joined up, (2) the onset of the intermittent bursting of secondary flows, leading to the 3/2I regime, and (3) where the drift period of mode $m = 3$ in the 3MAV-r regime diverged. This abundance of homoclinic behaviour, which might have some relevance to low-frequency variability observed in the atmosphere, was in contrast to the striking absence of secondary Hopf bifurcations in both generic flows as well as frequency locked flows. Rather, the transition from steady waves to vacillating waves led directly to weakly chaotic flow on a complex 'fuzzy' torus, and it appeared that quasi-periodic flow on a torus was restricted to those flows which showed marked phase coherence in the harmonic triads, i.e. 2+3IV and 3AV. The torus of the 2+3IV flow was then observed to undergo a torus-doubling bifurcation before breaking up completely to the D_2 flow.

The widely observed frequency locking of the modulation frequency to the drift frequency did not seem to affect the bifurcation structure, but complete locking of the modulation, drift, and vacillation frequencies resulted in period-doubling as the preferred bifurcation. The homoclinic orbit seemed to persist in frequency locked flows which led to flows consistent with intermittency type-III in the 3/2I regime, while the generic 3/2I flow was consistent with either type-I or type-II intermittency.

We suggest that the weak coupling of the travelling waves with the container might be an important factor which might account for the frequently observed discrepancies between numerical models and laboratory experiments. It is planned to study the effect of this coupling mechanism in a series of experiments using controlled perturbations of the cylindrical symmetry in the apparatus combined with some low-order models, which include zonally non-uniform forcing.

Not all flows seemed to be consistent with low-dimensional dynamics, but flows involving structural vacillation (2SV and 2-3A) showed apparently stochastic behaviour, which might be the transient growth of 'non-normal' modes from a localized instability. These perturbations might be akin to the optimal modes known in atmospheric instability theory, which do not preserve shape during their growth. In this case the study of the structure of the SV flows requires a high resolution three-dimensional flow visualization technique. The effect of these small fluctuations on the bifurcations, however, could be modelled either by a purely deterministic model where the SV modes are higher radial normal modes, or by a purely stochastic parametrization of the SV in the form of random forcing.

A fundamental aspect of these experiments is the simple geometry of the apparatus, which helps in the investigation of the fundamental physical processes discussed above. Future research, of course will have to address the implications of these sym-

metric systems to the more complex situations as flows in the atmosphere or in oceans. A step towards these situations would be to study baroclinic instability in an open system such as a straight channel geometry with inflow and outflow at either end of the straight channel section. In this case, the flow would not be subjected to the azimuthal periodicity condition.

We thank Professor Raymond Hide for his support and encouragement during the course of this work, as well as for many inspiring discussions. We are also grateful to Dr Tom Mullin and Dr Patrice Klein for helpful comments and discussions. The help from Mr Mike Buckler in modifying the apparatus is greatly appreciated. The work was partly funded in the early stages by the UK Meteorological Office and later by the NERC. W.-G.F. is grateful for a studentship provided by the European Communities Commission.

Appendix A. Phase locking

From the integrated resonance condition for wave triads (equation (2.3)),

$$\varphi_{m-m'-m''} \equiv \phi_m - \phi_{m'} - \phi_{m''} \approx \text{const.}, \tag{A 1}$$

one can evaluate a time-averaged quantity which shows how often each value of φ (between 0 and 2π) is assumed by $\varphi_{m-m'-m''}(t)$. This 'locking density', $\rho_{m-m'-m''}$, may be defined as the probability density function $\rho(\varphi_{m-m'-m''})d\phi$ over the data set, and gives information about the time-averaged phase locking: strong phase coherence would result in a strong peak at the preferred value of φ, while no phase coupling would give a fairly flat density function over its entire range $0 \ldots 2\pi$.

If no amplitude dependence needs to be considered then the phase locking function $\varphi_{m-m'-m''}$ at time t makes a non-zero contribution to $\rho_{m-m'-m''}$ only at $\phi = \varphi_{m-m'-m''}$. This can be expressed with the delta function, $\delta\left(\phi - \varphi_{m-m'-m''}(t)\right)$, which then is integrated over time and normalized by all contributions (i.e. the limits of the time integration):

$$\rho^*_{m-m'-m''}(\phi) = \frac{1}{t_e - t_0} \int_{t_0}^{t_e} \mathrm{d}t\, \delta(\phi - \varphi_{m-m'-m''}(t)). \tag{A 2}$$

If one needs to separate the contribution from different amplitude ranges of the participating modes, then at each time the contribution to the locking density has to be weighted, either by 1 if all three modes are within their preselected amplitude window, or by 0 otherwise. This weighting is achieved by multiplying $\delta\left(\phi - \varphi_{m-m'-m''}(t)\right)$ by two Heaviside functions, H, for each mode j, one setting the lower limit of the amplitude window and one the higher limit: $H(A_j(t) - A_j^{\min})H(A_j^{\max} - A_j(t))$. In the following equation this weighting is applied also to the normalization factor to ensure $\int \rho\, \mathrm{d}\phi = 1$. With these amplitude windows, equation (A 2) becomes

$$\rho^*_{m-m'-m''}(\phi; \{A_j^{\min,\max}\}) = \frac{\int_{t_0}^{t_e} \mathrm{d}t \delta(\phi - \varphi_{m-m'-m''}(t)) \prod_j H(A_j(t) - A_j^{\min})H(A_j^{\max} - A_j(t))}{\int_{t_0}^{T} \mathrm{d}t \prod_j H(A(t) - A_j^{\min})H(A_j^{\max} - A_j(t))}, \tag{A 3}$$

where $j = m, m', m''$ and

$$H(x) = \begin{cases} 1 & \text{if } x \geqslant 0, \\ 0 & \text{otherwise.} \end{cases}$$

In practice, $\rho_{m-m'-m''}$ is calculated by counting the scans for which

$$\phi \leqslant \varphi_{m-m'-m''} < \phi + \delta\phi,$$

provided the amplitudes of the waves are within a preselected amplitude range. The density is normalized to have unit area in the interval $0 \ldots 2\pi$:

$$\rho_{a-b-c}(\phi) = \frac{1}{\delta\phi} \times \frac{\text{no. of scans with } \left\{ \begin{array}{l} \phi \leqslant \varphi_{a-b-c} < \phi + \delta\phi, \text{ and} \\ A_j^{min} \leqslant A_j \leqslant A_j^{\max}, j = a, b, c \end{array} \right\}}{\text{no. of scans with } \{A_j^{min} \leqslant A_j \leqslant A_j^{\max}, j = a, b, c\}}. \quad \text{(A 4)}$$

As in the triad phase locking a sideband locking probability density, ρ_m can be defined as a measure of the time-averaged strength of the wave coupling by this mechanism with equation (A 4), but using Φ_m instead of $\varphi_{m-m'-m''}$.

References

Aubry, N., Holmes, P., Lumley, J. L. & Stone, E. 1988 The dynamics of coherent structures in the wall region of a turbulent boundary layer. *J. Fluid Mech.* **192**, 115–173.

Benjamin, T. B. & Feir, J. E. 1967 The disintegration of wavetrains on deep water. I. Theory. *J. Fluid Mech.* **27**, 417–430.

Birchfield, G. E. & Ghil, M. 1992 Climate evolution in the Pliocene and Pleistocene from marine-sediment records and simulations: internal variability versus orbital forcing. *J. Geophys. Res.* D **98**, 10385–10399.

Bretherton, F. P. 1964 Resonant interactions between waves. The case of discrete oscillations. *J. Fluid Mech.* **20**, 457–479.

Broomhead, D. S. & King, G. P. 1986 Extracting qualitative dynamics from experimental data. *Physica* D **20**, 217–236.

Buzyna, G., Pfeffer, R. L. & Kung, R. 1984 Transitions to geostrophic turbulence in a rotating differentially heated annulus of fluid. *J. Fluid Mech.* **145**, 377–403.

Collins, M., Lewis, S. R. & Read, P. L. 1995 Regular and irregular baroclinic waves in a martian general circulation model: a role for diurnal forcing. *Adv. Space. Res.* **16**(6), 3–7.

Condon, E. U. & Odishaw, H. 1985 *Handbook of physics*. New York: McGraw-Hill.

Craik, A. D. D. 1985 *Wave interactions and fluid flows*. Cambridge and New York: Cambridge University Press.

Darbyshire, A. G. & Price, T. J. 1991 Phase portraits from chaotic time series. *Fractals and chaos* (ed. A. J. Crilly, R. A. Earnshaw & H. Jones), pp. 247–258. Berlin and Heidelberg: Springer.

Egger, J. & Schilling, H.-D. 1983 On the theory of the long-term variability of the atmosphere. *J. Atmos. Sci.* **83**, 1073–1085.

Farrell, B. F. 1989 Optimal excitation of baroclinic waves. *J. Atmos. Sci.* **46**, 1193–1206.

Fowlis, W. W. & Pfeffer, R. L. 1969 Characteristics of amplitude vacillation in a rotating, differentially heated fluid annulus determined by a multi-probe technique. *J. Atmos. Sci.* **26**, 100–108.

Früh, W.-G. 1996 Low-order models of wave interactions in the transition to baroclinic chaos. *Nonlin. Proc. Geophys.* **3**, 150–165.

Gaveau, B., Gudowska-Nowak, E., Kapral, R. & Moreau, M. 1992 Stochastic transitions between a limit cycle and a fixed point. *Physica* A **188**, 443–451.

Ghil, M. 1994 Cryothermodynamics: the chaotic dynamics of paleoclimate. *Physica* D **77**, 130–159.

Grassberger, P. & Procaccia, I. 1983 Characterization of strange attractors. *Phys. Rev. Lett.* **50**, 346–349.

Grebogi, C., Ott, E., Romeiras, F. & Yorke, J. A. 1987 Critical exponents for crisis-induced intermittency. *Phys. Rev.* A **36**, 5365–5380.

Guckenheimer, J. & Buzyna, G. 1983 Dimension measurements for geostrophic turbulence. *Phys. Rev. Lett.* **51**, 1438–1441.

Hart, J. E. 1981 Wavenumber selection in nonlinear baroclinic instability. *J. Atmos. Sci.* **38**, 400–408.

Hasselmann, K. 1976 Stochastic climate models. I. Theory. *Tellus* **28**, 473–485.

Hide, R. 1953 Some experiments on thermal convection in a rotating liquid. *Q. J. R. Met. Soc.* **79**, 161.

Hide, R. 1958 An experimental study of thermal convection in a rotating liquid. *Phil. Trans. R. Soc. Lond.* A **250**, 441–478.

Hide, R. & Mason, P. J. 1975 Sloping convection in a rotating fluid. *Adv. Phys.* **24**, 47–99.

Hide, R. & Mason, P. J. 1978 On the transition between axisymmetric and non-axisymmetric flow in a rotating liquid annulus subject to a horizontal temperature gradient. *Geophys. Astrophys. Fluid Dyn.* **10**, 121–156.

Hide, R., Mason, P. J. & Plumb, R. A. 1977 Thermal convection in a rotating fluid subject to a horizontal temperature gradient: spatial and temporal characteristics of fully developed baroclinic waves. *J. Atmos. Sci.* **34**, 930–950.

Hignett, P. 1985 Characteristics of amplitude vacillation in a differentially heated rotating fluid annulus. *Geophys. Astrophys. Fluid Dyn.* **31**, 247–281.

Hignett, P., White, A. A., Carter, R. D., Jackson, W. D. N. & Small, R. M. 1985 Comparison of laboratory measurements and numerical simulations of baroclinic wave flows in a rotating cylindrical annulus. *Q. J. R. Met. Soc.* **111**, 131–154.

James, I. N. & James, P. M. 1989 Ultra-low-frequency variability in a simple atmospheric circulation model. *Nature* **342**, 53–55.

James, I. N. & James, P. M. 1992 Spatial structure of ultra-low-frequency variability of the flow in a simple atmospheric circulation model. *Q. J. R. Met. Soc.* **118**, 1211–1233.

James, I. N., Jonas, P. R. & Farnell, L. 1981 A combined laboratory and numerical study of fully developed steady baroclinic waves in a cylindrical annulus. *Q. J. R. Met. Soc.* **107**, 51–78.

James, P. M., Fraedrich, K. & James, I. N. 1994 Wave-zonal-flow interaction and ultra-low-frequency variability in a simplified global circulation model. *Q. J. R. Met. Soc.* **120**, 1045–1067.

Jonas, P. R. 1981 Some effects of boundary conditions and fluid properties on vacillation in thermally driven rotating flow in an annulus. *Geophys. Astrophys. Fluid Dyn.* **18**, 1–23.

Kaiser, J. A. C. 1970 Rotating deep annulus convection. 2. Wave instabilities, vertical stratification and associated theories. *Tellus* **22**, 275–287.

Lorenz, E. N. 1990 Can chaos and intransitivity lead to interannual variability. *Tellus* **42A**, 378–389.

Mansbridge, J. V. 1984 Wavenumber transition in baroclinically unstable flows. *J. Atmos. Sci.* **41**, 925–930.

Moroz, I. M. & Holmes, P. 1984 Double Hopf bifurcation and quasi-periodic flow in a model for baroclinic instability. *J. Atmos. Sci.* **41**, 3147–3160.

Mundt, M. D., Brummell, N. H. & Hart, J. E. 1995 Linear and nonlinear baroclinic instability with rigid sidewalls. *J. Fluid Mech.* **291**, 109–138.

Ohlsen, D. R. & Hart, J. E. 1989*a* Transitions to baroclinic chaos on the β-plane. *J. Fluid Mech.* **203**, 23–50.

Ohlsen, D. R. & Hart, J. E. 1989*b* Nonlinear interference vacillation. *Geophys. Astrophys. Fluid Dyn.* **45**, 213–235.

Pedlosky, J. 1981 The nonlinear dynamics of baroclinic wave ensembles. *J. Fluid Mech.* **102**, 169–209.

Pfeffer, R. L. & Fowlis, W. W. 1968 Wave dispersion in a rotating, differentially heated cylindrical annulus of fluid. *J. Atmos. Sci.* **25**, 361–371.

Pfeffer, R. L., Buzyna, G. & Kung, R. 1980 Time-dependent modes of thermally driven rotating fluids. *J. Atmos. Sci.* **37**, 2129–2149.

Pielke, R. A. & Zeng, X. 1994 Long-term variability of climate. *J. Atmos. Sci.* **51**, 155–159.

Plaut, G. & Vautard, R. 1994 Low-frequency oscillations and weather regimes in the northern hemisphere. *J. Atmos. Sci.* **51**, 210–236.

Plumb, R. A. 1977 The stability of small amplitude Rossby waves in a channel. *J. Fluid Mech.* **80**, 705–720.

Rand, D. 1982 Dynamics and symmetry: predictions for modulated waves in rotating fluids. *Arch. Ration. Mech. Analysis* **79**, 1–37.

Read, P. L. 1993 Phase portrait reconstruction using multivariate singular systems analysis. *Physica* D **69**, 353–365.

Read, P. L., Bell, M. J., Johnson, D. W. & Small, R. M. 1992 Quasi-periodic and chaotic flow regimes in a thermally-driven, rotating fluid annulus. *J. Fluid Mech.* **238**, 599–632.

Rind, D. & Overpeck, J. 1993 Hypothesized causes of decade-to-century-scale climate variability: climate model results. *Q. Sci. Rev.* **12**, 357–374.

Schuster, H. G. 1989 *Deterministic chaos* 2nd edn. Weinheim: VCH Verlagsgesellschaft.

Smith, L. A. 1992 Identification and prediction of low dimensional dynamics. *Physica* D **58**, 50–76.

Sommerer, J. C., Ditto, W. L., Grebogi, C., Ott, E. & Spano, M. L. 1991 Experimental confirmation of the scaling theory for noise-induced crises. *Phys. Rev. Lett.* **66**, 1947–1950.

Strong, C., Jin, F.-F. & Ghil, M. 1995 Intraseasonal oscillations in a barotropic model with annual cycle, and their predictability. *J. Atmos. Sci.* **52**, 2627–2642.

Tamaki, K. & Ukaji, K. 1993 Characteristics of tilted-trough vacillation in a differentially heated rotating fluid annulus. *J. Met. Soc. Jap.* **71**, 553–566.

Ukaji, K. & Tamaki, K. 1990 A numerical study of tilted-trough vacillation observed in a differentially heated rotating fluid annulus. *J. Met. Soc. Jap.* **68**, 447–460.

Weng, H.-Y., Barcilon, A. & Magnan, J. 1986 Transitions between baroclinic flow regimes. *J. Atmos. Sci.* **43**, 1760–1777.

Wolf, A., Swift, J. B., Swinney, H. L. & Vastano, J. A. 1985 Determining Lyapunov exponents from a time series. *Physica* D **16**, 285–317.

Received 14 November 1995; revised 25 June 1996; accepted 17 July 1996